UNIVERSITÉ DE LAUSANNE - FACULTÉ DES SCIENCES

Conductivité thermique des supraconducteurs dans l'état intermédiaire: effet de dimension dans une structure lamellaire longitudinale

RÉSUMÉ DE LA THÈSE DE DOCTORAT
présentée à la Faculté des Sciences de l'Université de Lausanne

par

Jean-Marc SUTER
Physicien diplômé
Licencié ès sciences mathématiques

1976

Imprimerie A. Groux
Avenue de Morges 9
1004 Lausanne

1975

Digitized by the Internet Archive
in 2026

https://archive.org/details/IA41546820_0035

UNIVERSITÉ DE LAUSANNE - FACULTÉ DES SCIENCES

Conductivité thermique des supraconducteurs dans l'état intermédiaire: effet de dimension dans une structure lamellaire longitudinale

RÉSUMÉ DE LA THÈSE DE DOCTORAT
présentée à la Faculté des Sciences de l'Université de Lausanne

par

Jean-Marc SUTER
Physicien diplômé
Licencié ès sciences mathématiques

Imprimerie A. Groux
Avenue de Morges 9
1004 Lausanne

1975

Imprimatur

Université de Lausanne
Faculté des Sciences

Vu le rapport présenté par le jury d'examen, composé de

MM les Professeurs Léo RINDERER, directeur de thèse, François ROTHEN et Jörgen OLSEN, experts, et Robert HUGUENIN, président du jury

le Conseil de Faculté autorise l'impression de la thèse de

M. Jean-Marc SUTER, physicien diplômé et licencié ès sciences mathématiques

intitulée "CONDUCTIVITE THERMIQUE DES SUPRACONDUCTEURS DANS L'ETAT INTERMEDIAIRE : EFFET DE DIMENSION DANS UNE STRUCTURE LAMELLAIRE LONGITUDINALE"

Lausanne, le 12 janvier 1976

pour *Le doyen de la Faculté des Sciences:*
Robert HUGUENIN, vice-doyen

R. Huguenin

UNIV.
LEIDEN
BIBL.

Ce tiré à part est le résumé de la thèse présentée dont un texte dactylographié complet peut être consulté à la Bibliothèque cantonale et universitaire de Lausanne.

Journal of Low Temperature Physics, Vol. 31, Nos. 1/2, 1978

Thermal Conductivity of Superconductors in the Intermediate State: Size Effect in a Longitudinal Lamellar Structure*

J. M. Suter† and L. Rinderer

Institut de Physique Expérimentale, Université de Lausanne, Lausanne-Dorigny, Switzerland

(Received August 4, 1977)

The thermal conductivity of type I superconductors has been measured in a well-defined, optically controlled intermediate-state configuration, the so-called longitudinal lamellar structure (LLS). A regular arrangement of alternating normal and superconducting lamellas is obtained in an elongated plate by applying the magnetic field obliquely (following Sharvin) and decreasing it from the critical value. The heat current is set parallel to the lamellas. Due to the peculiar reflection law governing the quasiparticle reflections at a normal–superconductor interphase boundary, the thermal conductivity of the LLS is reduced when the electronic mean free path is larger than or comparable to the width of the lamellas. As first pointed out by Andreev, the reflection occurs with vector-momentum conservation, and only the quasiparticles moving nearly parallel to the lamellas can transport heat efficiently. The corresponding reduction of the thermal conductivity is a size effect.

Systematic measurements of the thermal conductivity of the LLS in high-purity lead and tin are interpreted in terms of the size-effect model. The parameters of the model were experimentally determined in a preliminary study, to enable an unambiguous comparison with the theory. In particular, the geometrical aspects of the structures were studied using a magnetooptical technique. Interesting results on the characteristics of the LLS were obtained. The thermal conductivity data on lead essentially confirm the size-effect description. In lead below 4.2 K, heat is conducted much more efficiently by the normal lamellas than by the superconducting ones. In particular, phonon effects in the superconducting phase can be neglected and the results give information on the behavior of the normal-phase quasiparticles. The situation is different for tin, where heat transport by the lamellas of both types takes place, the heat carriers being the electrons ($T \geqslant 1.6\,K$). The discrepancy

* Supported financially by the Fonds National Suisse de la Recherche Scientifique.

†Present address: Eidgenössisches Institut für Reaktorforschung, 5303 Würenlingen, Switzerland.

0022-2291/78/0400-0033$05.00/0 © 1978 Plenum Publishing Corporation

between the predictions of the size-effect model and the observed values in tin are attributed to an oversimplified calculation of the contribution of the superconducting lamellas to the conductivity. A more detailed treatment is needed, but the basic description of the thermal conductivity reduction in terms of the size effect should remain.

1. INTRODUCTION

The intermediate-state thermal conductivity was used in early studies of the properties of the normal (N) to superconductor (S) interphase boundaries (see, e.g., Refs. 1–3). The first anomaly was discovered in 1950 by Mendelssohn and Olsen,[4] who found in the intermediate state a lower thermal conductivity than in both the N and S states.

In the case of dominant phonon conductivity in the superconducting domains, it was shown by Laredo and Pippard[5] that the anomalously small conductivity can be explained by the reduction of the effective phonon mean free path (mfp) in the S phase introduced by the adjacent normal domains, in which the phonon mfp is much smaller. The effective phonon mfp in the S domains is then comparable to the size of these domains. The electronic conductivity can be neglected as a consequence of the drastic reduction of the number of excitations in the S phase below T_c. An alternative explanation was proposed by Cornish and Olsen,[6] who pointed out that imperfect thermal relaxation between electrons and lattice would also lead to a conductivity minimum in the intermediate state.*

When heat conduction by electrons is the dominant mechanism in both the N and S phases, an additional resistance arising from excitation scattering by interphase boundaries had to be introduced to account for the low thermal conductivity in the intermediate state. Measurements of this quantity thus turned out to be a useful tool in the investigation of the behavior of the excitations at the N–S boundaries (see, e.g., Refs. 2 and 3). However, progress in this study was restrained by one fundamental experimental difficulty, which had been already encountered in early work: The thermal conductivity curves, recorded at constant temperature as a function of the applied field, display hysteresis. Thus, only certain aspects of the data could be used in the interpretation of the results. Generally, the selected feature was the amplitude of the thermal resistivity maximum obtained in increasing the field starting from the S state. A global model,[8] i.e., a model in which any geometrical detail in the intermediate-state structure is ignored, succeeded in describing the temperature and sample-size dependencies of that maximum.[3,7]

* More details on the case of dominant phonon conductivity can be found, e.g., in Ref. 7.

Obviously, the thermal conductivity of a heterogeneous structure whose two components may have very different conductivities and in which, moreover, a boundary resistance may exist depends strongly on the geometry of the structure. This geometry has been extensively studied using optical techniques: The magnetic field distribution at the sample surface is "revealed" by a diamagnetic or ferromagnetic powder spread on the sample (see, e.g., Refs. 9–12), or by high-resolution magnetooptical techniques (see, e.g., Refs. 13–15). An important result for the understanding of the hysteresis in the thermal conductivity is the existence of very different intermediate-state structures depending on whether the applied field is increased from the S state or decreased from the N state: In the first case, normal flux tubes are surrounded by a superconducting matrix, whereas in the second one, superconducting lamellas in a normal matrix are obtained.[11]

Clearly, special care has to be taken to set up an intermediate-state structure of well-known form, as assumed, for example, in the nonglobal models of the intermediate-state thermal conductivity.[5,6,16,17] A sophisticated way of setting up the structure has been developed by Walton[18] from thermal and electrical conductivity measurements; however, no direct observation of the resulting structure was made. In the present work, we report the first extensive study of the thermal conductivity of a well-defined, optically controlled intermediate-state structure. The selected configuration consists of long, parallel lamellas, alternately superconducting and normal, extending from one end of an elongated plate to the other (Fig. 1). Such a structure, which will be called a *longitudinal lamellar structure* (LLS), can be obtained by Sharvin's slanting field method[9] under certain conditions (see Section 4). The thermal conductivity of the LLS when the heat flow is parallel to the general direction of the structure has been calculated by Andreev.[17] This quantity is anomalously small when the mfp of the heat carriers—the electronic excitations—exceeds the period of the structure. This is a consequence of the peculiar way in which the excitations are reflected by the N–S interphase boundaries.[16]

As first pointed out 1964 by Andreev, reflection of the excitations at the N–S interphase boundary occurs with energy and *vector*-momentum conservation, while the character of the quasiparticule changes (an incident electronlike excitation is reflected as a holelike one, and vice versa).[16] The recognition of this peculiar reflection gave a new impetus to the study of the N–S interphase boundaries. Many new interesting properties have been both theoretically predicted and experimentally observed. Besides the effect we are concerned with in the present paper, let us mention in particular the absence of additional boundary resistance in the case of an electrical current,[18–21] the existence of bound states in the N domains in the

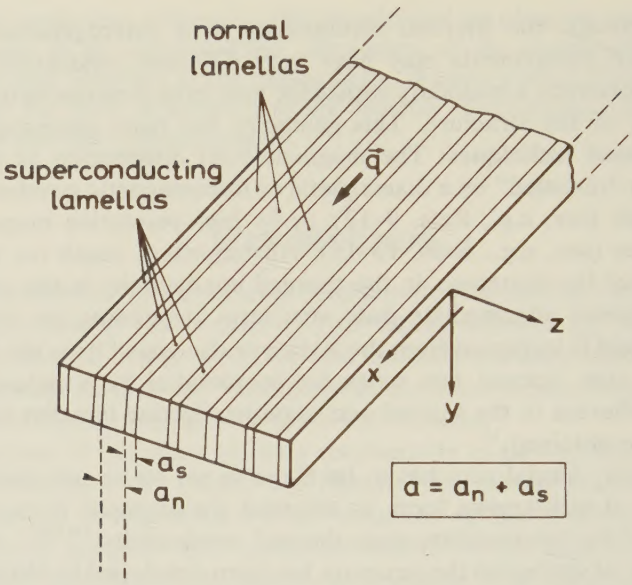

Fig. 1. The intermediate-state geometry considered in the present paper, the so-called longitudinal lamellar structure (LLS) in a long rectangular plate. The heat is flowing parallel to the lamellas, which are alternately superconducting and normal. The whole structure is static. The origin of the coordinate system is located at the center of the lamella, the thermal conductivity of which is calculated.[17]

intermediate state,[22,23] the Tomasch effect,[24,25] and a special radio-frequency size effect in the intermediate state.[26,27] All these effects confirmed the correctness of Andreev's picture.

The size effect affecting the thermal conductivity of the LLS is simple to understand. As the direction of propagation is conserved by the reflection process, the excitations are trapped between two adjacent interphase boundaries, provided their mfp is larger than or comparable to the width of the lamella. Only those excitations moving nearly parallel to the boundaries can contribute to the transport of heat along the LLS, i.e., the thermal conductivity is reduced by the boundary condition. The number of excitations that are left for heat transport decreases with increasing mfp or decreasing lamella width, and the effect described is a size effect.

Experimental evidence for the existence of the size effect in the thermal conductivity of the LLS has been reported elsewhere.[28] Some measurements on a high-purity lead sample were interpreted using an extension of Andreev's model of the size effect. Later, other partial results on lead and tin were briefly reported.[29] The present paper gives a complete

analysis of the results on these two metals. Theoretical aspects are first presented (Section 2). The experimental procedure is given in Section 3. Section 4 contains a study of the LLS, while Section 5 is devoted to the thermal conductivity data.

The data on lead are nicely interpreted in terms of the size effect model applied to the normal lamellas. These lamellas conduct heat much better than the S lamellas below 4.2 K, and the interpretation of the data can be restricted to the study of the electronic excitations in the N phase. In particular, phonon conduction in the S phase is unimportant.

For tin, the predictions of the size effect model deviate systematically from the experimental results. The deviation is traceable to the contribution of the S lamellas to the thermal conductivity. This contribution, mainly electronic above 1.6 K, was originally neglected by Andreev; it is much larger in the case of tin than for lead. In the extension of Andreev's model of Ref. 28 that is used in the interpretation of the data, the conductivity of the S lamellas is calculated too crudely.

2. THEORETICAL ASPECTS

In this section we give an outline of Andreev's model of the thermal conductivity of the LLS,[17] together with some extensions of this model.[28] The presentation is restricted to the elements needed in the interpretation of the experimental results of the next sections.

The calculation of the thermal conductivity of the LLS in the most general case is quite a difficult task. A certain number of simplifying assumptions will be considered in the following. In particular, the normal and the superconducting lamellas will be treated independently from one another. Their contributions to the thermal conductivity of the LLS will be added after appropriate scaling by the concentrations of the two phases. Concerning the effect of the magnetic field in the normal lamellas, only two limiting cases will be considered. The more general case in which the magnetoresistance and the size effect are simultaneously present in the N lamellas is beyond the scope of the present paper.

Finally, a set of three equations [Eqs. (5)–(7)] will be obtained, which we shall use throughout the paper to analyze the experimental results. The first equation corresponds to the low-field limit (electronic cyclotron radius much greater than lamella width); the size effect is present in both the S and N lamellas. The second equation describes just the opposite case, the high-field limit, in which the size effect is present only in the S lamellas, while the magnetoresistance replaces the size effect in the N lamellas. The last equation corresponds to the short-mfp limit, where each lamella has a

conductivity just equal to the bulk conductivity of the corresponding phase.

Andreev's calculation starts from the kinetic equation for the distribution function $n(\boldsymbol{r}, \boldsymbol{p})$ of the excitations. This equation is solved making the following assumptions: (i) low temperature compared to the critical temperature, $T \ll T_c$; (ii) low magnetic field, i.e., $r_c \gg l_h$, a_N [r_c is the cyclotron radius in a critical field $H_c(T)$, l_h is the mfp of the heat carriers*, and a_N is the width of the N lamellas of the LLS]. Consequently, heat conduction by the S lamellas is neglected, and the main contribution to the thermal conductivity is given by the electrons in the N lamellas. Moreover, no reference is made to the magnetic field in the kinetic equation.

The boundary condition to be used arises from Andreev's reflection law[16]: $n(\mathbf{n}, \xi) = n(\mathbf{n}, -\xi)$ at $z = \pm a_N/2$. Here, $\mathbf{n}$ is a unit vector in the direction of the excitation momentum $\mathbf{p}$, $\mathbf{n} = \mathbf{p}/p$, and ξ is the distance (in energy) from the Fermi level ($\xi > 0$ corresponds to an electronlike excitation, $\xi < 0$ to a holelike one). The axis disposition is given in Fig. 1. The boundary condition, which is justified by the assumption $T \ll T_c$, states that *all* the excitations are reflected with energy and vector momentum conservation and excitation character reversal.

The resulting distribution function is

$$n(\mathbf{n}, \xi) = n_0 - \frac{\partial n_0}{\partial T} \Lambda n_\alpha \frac{\partial T}{\partial x_\alpha} \left[1 - \frac{\exp(-z/\Lambda n_z)}{\cosh(a_N/2\Lambda n_z)} \right] \tag{1}$$

Here, $\Lambda = v\tau \operatorname{sgn}(\xi)$ is a signed, energy-dependent mfp, $v(\xi)$ being the group velocity of the excitations and τ their relaxation time caused by the scattering by impurities, lattice point defects, etc. In (1), $n_0 = [\exp(|\xi|/k_B T) + 1]^{-1}$ is the equilibrium distribution function of the excitations. The index α takes on the values x and y. The temperature T is assumed to be independent of z.

The mean heat current density and the thermal conductivity tensor $K_{\alpha\beta}$ in the (x, y) plane are then calculated in the usual way. The average is taken over one period a of the intermediate state structure. It is assumed, finally, that the mfp greatly exceeds the width of the N lamellas, and the limit $v\tau \to \infty$ is taken. The final result looks promising from the point of view of the Fermi surface study:

$$K_{\alpha\beta} \propto T(a_N^2/a) B_{\alpha\beta}$$

The tensor $B_{\alpha\beta}$ depends on the Gaussian curvature of the Fermi surface,[17] and also enters the calculation of the anomalous skin effect. This effect and

* The notation l_h recalls that the mfp for heat conduction is to be used, and not the one defined by electrical conductivity measurements.

the effect studied in this paper have the common feature that the main contribution is given by electrons moving nearly parallel to a certain plane.

Experimentally, the limiting situation considered by Andreev is difficult to approach. The most restrictive condition is that of a very long mfp compared to the width a_N of the lamellas. In a plate of thickness d, $a_N \propto \sqrt{d}$,[30] and $a_N \approx 10^{-1}$ mm for $d = 1$ mm (Section 4). Reducing the thickness d reduces a_N only slowly and has two additional disadvantages: (i) The condition $a_N \ll d$, which is implicit in the above calculation, is no longer fulfilled; (ii) the bulk mfp l_h is no longer smaller than d, and "ordinary" size effects, i.e., effects arising from collisions of electrons with the sample surface, complicate the interpretation. On the other hand, it is difficult to get an electronic mfp larger than ~ 1 mm, even using very pure material. Thus, typical values of the ratio l_h/a_N are 10 or less. In the simplest case of a spherical Fermi surface, it is easy to calculate the l_h/a_N dependence of the conductivity from Andreev's expression (see below).

Another restrictive assumption made by Andreev is that of the low magnetic field. Here, no degree of freedom is left to the experimentator since, for a given material, (i) the field in a N lamella always is equal to $H_c(T)$, and (ii) the width a_N of such a lamella is imposed by the sample thickness (see above).* From the point of view of the theoretician, it is difficult to account for the effect of the field in a detailed manner. We shall only consider two limiting cases: Andreev's low-field limit, and the opposite case, the high-field limit $r_c \ll a_N$. In the latter case, the excitation trajectories are bent in such a way that excitation trapping between two parallel N–S interphase boundaries is no longer possible. Andreev's size effect is then inhibited, while magnetoresistance is enhanced. We see that the magnetoresistance and the size effect studied in this paper are competitive phenomena. In the two limiting cases just mentioned, only one effect is present. However, real situations may correspond to intermediate cyclotron-radius values, where both effects are present; the calculation is then much more complicated and is not considered by us.

In the interpretation of the results on tin, heat conduction by the S lamellas has to be taken into account, unlike in Andreev's model (see Section 5). Andreev's calculation can be easily extended to the S lamellas of the LLS if one additional assumption is made, namely that *all* the excitations of the S phase are reflected by the interphase boundaries.[28] This is a rather drastic assumption, as will be seen in Section 5, because the excitations of the S phase do not see a potential well, as do those of the N phase. However, one can show that the transmission probability is very small if the energy is equal to the superconducting energy gap, hence for

*The field dependence of a_N is the same for all thicknesses.

most excitations of the S phase.[31,*] Making the additional assumption greatly simplifies the calculation of the thermal conductivity. The contributions of the two phases can be calculated separately, and then added after scaling by the concentrations.[28]

The following modifications have to be introduced in Andreev's calculation in order to obtain the contribution of the S phase in the above approximation: (i) The BCS excitation spectrum and group velocity replace the corresponding quantities of the N phase; thus, the new value of Λ in Eq. (1) is

$$\Lambda_S = \frac{|\xi|}{E} v_F \left(\frac{1}{\tau_{ph}} + \frac{|\xi|}{E} \frac{v_F}{l_i} \right)^{-1} \operatorname{sgn}(\xi)$$

Here, $E = (\xi^2 + \Delta^2)^{1/2}$ where $\Delta(T)$ is the superconducting energy gap; v_F is the Fermi velocity (the Fermi surface is assumed to be spherical); τ_{ph} is the relaxation time for scattering of electrons by phonons; and l_i is the mfp for scattering of electrons by impurities. Both τ_{ph} and l_i have in the S lamellas the same values as in the N lamellas.[32,33] (ii) In the calculation of the mean heat current along a S lamella the average has to be taken over the width a_S of this lamella. Neglecting the T dependence of Δ in the calculation of $\partial n_0 / \partial T$, one obtains[28]

$$\begin{aligned} K_{\alpha\beta} &= \delta_{\alpha\beta} K_S(T, a_S) \\ K_S(T, a_S) &= A \int_\delta^\infty g(t) \Theta[(a_s/2l_i) w(t)] \, dt \\ g(t) &= \frac{t^2 e^t}{(e^t + 1)^2 w(t)} \\ w(t) &= 1 + (l_i / v_F \tau_{ph})[1 - (\delta/t)^2]^{-1/2} \end{aligned} \tag{2}$$

with $A \propto T l_i$ and $\delta = \Delta(T)/k_B T$. The function

$$\Theta(\zeta) = \frac{3}{2} \zeta \int_\zeta^\infty \left[1 - \left(\frac{\zeta}{u} \right)^2 \right] \left(1 - \frac{\tanh u}{u} \right) \frac{du}{u^2}$$

was calculated numerically (Fig. 2). Andreev used its asymptotic form $\Theta(\zeta) \propto \zeta$ for $\zeta \to 0$ (see dashed line through the origin of Fig. 2).

The coefficient A, which contains the Fermi momentum, can be eliminated in taking the ratio

$$R_S(T, a_S) = K_S(T, a_S) / [\lim_{a_S \to \infty} K_S(T, a_s)] \tag{3}$$

the denominator of which is equal to the bulk conductivity $K_S(T)$ of the

*Here, the possibility for the excitations of the S phase to tunnel through a N lamella is ignored, although this process could be important (see Section 5).

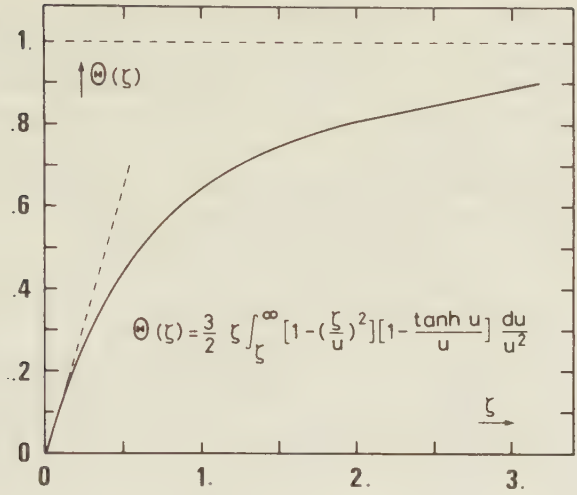

Fig. 2. Characteristic function of the size effect affecting the thermal conductivity of the LLS. The calculation is made assuming low magnetic field, spherical Fermi surface, and reflection of all the quasiparticles by the interphase boundaries. The variable ζ is related to the ratio of the electronic mfp to the width of the lamella considered. See text. The dashed lines represent the asymptotic form considered by Andreev[17] ($\zeta \to 0$) and the short-mfp limit ($\zeta \to \infty$).

sample in the S state. Thus, $R_S(T, a_S)$ is the relative conductivity of a S lamella with size effect.

In the same approximation, the relative conductivity of a N lamella with size effect—the normalization being made with respect to $K_N(T, H = 0)$, the N-state thermal conductivity extrapolated to zero field—is readily obtained by putting $\Delta = 0$ in (2):

$$R_N(T, a_N) = \Theta\left[\frac{a_N}{2}\left(\frac{1}{l_i} + \frac{1}{v_F \tau_{ph}}\right)\right] \tag{4}$$

Thus, the physical meaning of the function Θ is straightforward: Θ describes the thermal conductivity reduction due to the size effect in a N lamella; as expected, its argument is a function of the ratio l_h/a_N of the mfp over the lamella width.

In the two limiting cases mentioned above, the conductivity of the LLS is the following. In the *low-field limit* ($r_c \gg a_N$), the size effect is taken into account in both the N and S lamellas:

$$K(T, x_N) = x_N R_N(T, a_N) K_N(T, H = 0) + (1 - x_N) R_S(T, a_S) K_S(T) \tag{5}$$

with $a_N = x_N a(T, x_N)$ and $a_S = (1 - x_N) a(T, x_N)$. Here x_N is the concentration of the N phase and $a(T, x_N)$ is the period of the LLS. The terms R_N and R_S are given by Eqs. (2)–(4). In Eq. (5) there is no adjustable parameter, since all quantities can be experimentally determined.

In the *high-field limit* ($r_c \ll a_N$), the only modification with respect to the above calculation is the replacement of the size effect by the magnetoresistance in the contribution of the N lamellas:

$$K(T, x_N) = x_N K_N[T, H_c(T)] + (1 - x_N) R_S(T, a_S) K_S(T) \tag{6}$$

$K_N[T, H_c(T)]$ is the measured, bulk conductivity in a critical field.

Finally, in the *short-mfp limit* ($l_h \to 0$), magnetoresistance and size effect are both negligible and Eqs. (5) and (6) both have the following equation as common limit:

$$K(T, x_N) = x_N K_N(T) + (1 - x_N) K_S(T) \tag{7}$$

3. EXPERIMENTAL DETAILS

3.1. Sample Preparation

The samples are elongated plates to meet the requirements of both measuring the thermal conductivity and producing the desired intermediate-state structure (see Section 4). All the samples are polycrystalline. Size and transport characteristics are given in Table I. The two purest samples, Pb 1 and Sn 1, were used to study the size effect, the less pure, Sn 2, being used as a reference.*

All samples were given their final form by rolling the supplied ingot to the desired thickness and then spark-cutting the sides to obtain sharp edges. The samples were etched at intermediate stages during this preparation. Sn 1 was subsequently annealed in vacuo at 210°C for 36 h to stabilize its low temperature transport properties.[34] It was not necessary to apply any heat treatment to Sn 2 and Pb 1, because Sn 2 was stable enough for the few measurements required on it,[34] and lead anneals rather quickly during room-temperature storage; for safety purposes, however, we stored Pb 1 for two months after preparation before beginning the measurements, and in any case no ageing effect was observed.

*Some results on Pb 1 have been already published in Ref. 28, and together with others on Sn 1, in Ref. 29. Sn 2 was also studied in Ref. 34.

TABLE I

Sample Characteristics

	Pb 1	Sn 1	Sn 2
Nominal purity, %	99.999+	99.99997	99.9
Supplier	ASARCO	Vulcan Detinning	Dr. Bender & Hobein, Zürich
Size, mm			
Thickness	0.905 ± 0.005	0.947 ± 0.005	1.038 ± 0.004
Width	9.82 ± 0.02	9.18 ± 0.07	10.15 ± 0.05
Length	111	108	107
Resistivity ratio $\rho_{293}/\rho_{4.15}$	16,000[a]	27,700	147[c]
Residual resistivity ratio ρ_{293}/ρ_0	~85,000[a]	~36,000[b]	147[c]

[a] Obtained by extrapolation to zero field. See Section 5.2.

[b] Also extrapolated to zero field from magnetoresistance measurements above the critical field.

[c] This value was measured after a 15-month storage at room temperature, during which a metallurgical transformation took place (impurity migration; see Ref. 34). The electrical resistance was found to be strongly dependent on the measuring current and on the applied magnetic field. The quoted value was obtained under saturating conditions. The inhomogeneities in the impurity concentration had no influence on the thermal conductivity of the sample, as was demonstrated by repeating the measurements made immediately after sample preparation.

3.2. Thermal and Electrical Conductivity Measurements

Both thermal and electrical conductivities are measured in the range 1.6–4.2 K with the same geometrical factor, using the apparatus represented in Fig. 3.

The thermal conductivity is determined by the stationary heat flow method, with temperature differences ~0.03 K. The precision of these measurements is about 3%, while the absolute accuracy is of the order of 5%. The resistance of the "cold" thermometer Th A and the difference of the resistance of the two well-matched Allen-Bradley 56-Ω, 1/8-W thermometers are measured.[36] For the latter measurements, Th A and Th B are mounted in two adjacent branches of a dc Wheatstone bridge, and a superconducting* Nb wire connects the resistors electrically but not thermally.

Care was taken to stabilize the characteristics of the resistors before mounting them into their small copper blocks; they were covered with

*The maximum field used is 1 kOe.

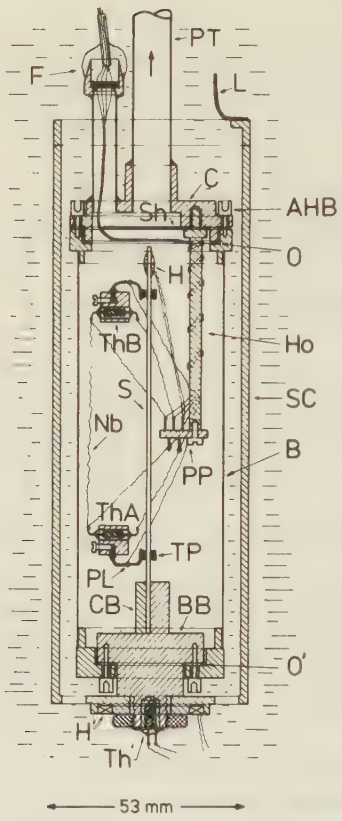

Fig. 3. Experimental device for thermal and electrical conductivity measurements. S, the sample, an elongated plate. H, main heater. Th A, Th B, thermometers (56-Ω Allen-Bradley resistors, epoxy-sealed in small copper blocks). TP, temperature probes. PL, potential leads. Nb, thin niobium wire. The sample is pressed by six phosphor-bronze Allen-head-bolts between the bottom block BB and the counter block CB. The temperature of BB is stabilized using the auxiliary thermometer Th′ and heater H.′ SC, squirrel cage for coaxial current return in electrical resistivity measurements. L, current lead (the other lead is soldered to the upper end of the sample, the vacuum box B being removed). O,O′, gold O-rings. C, top cover (copper). Sh, radiation shield. AHB, phosphor-bronze Allen-head-bolts. PP, pin plate with holder Ho (copper). F, epoxy-sealed electrical feedthrough (after Ref. 35). PT, pumping tube. For clarity, the sample holder, which prevents the sample from bending at room temperature, and the orientation control device (see Fig. 4) are not represented here.

epoxy (the original varnish being removed), and then 50 times cycled between room and liquid-nitrogen temperature; the two most stable and matched of 14 resistors were chosen; during the 25 subsequent thermal cycles required by the helium temperature measurements, their resistance changed by less than 0.3%.

The copper temperature probes TP surround the entire sample, so that the mean temperature on one cross section is measured, smoothing out any transverse thermal gradient. The potential leads are attached to the temperature probes with a low-melting-point solder.

The thermometers are calibrated against the vapor pressure of the helium bath in the absence of heat dissipation in the main heater H. By means of a least-squares fit, the coefficients of a calibration curve of the form[37] $X \ln R + Y/\ln R + Z = 1/T$ are then determined for each thermometer separately. For subsequent calculation of the thermal conductivity in the normal and superconducting states, the temperature calculated

with the calibration curves is used without correction (for magnetoresistance, hydrostatic head, etc.). A more accurate procedure is not needed in our case (see Section 5).

In the intermediate state, the thermal resistivity—or more precisely, a voltage whose variation is nearly proportional to that of the thermal resistivity—is recorded continuously as a function of the magnetic field. A constant power is dissipated in the heater H while the field is swept, the temperature of the block BB being kept constant. Care is taken to reduce to a minimum the variation of the mean temperature of the sample due to changes in its conductivity. The heat flow never exceeds 300 mW cm^{-2}—thus ensuring at the same time *static* intermediate-state structures[15] having reasonably small, longitudinal period and concentration gradients.* Moreover, the heat transfer between the sample and the helium bath is facilitated by (i) pressing the (soft) sample between the two pieces CB and BB, with silicon grease added to increase the surface of thermal exchange†; (ii) annealing the copper block BB for 5 h at 540°C in vacuo, and then cooling it slowly down to room temperature (12 h); (iii) extending the heat exchange surface to the bath in using also the bottom of the squirrel cage SC. The measured thermal conductance between the "cold" (Th A) and the auxiliary (Th′) thermometers is 0.7 W K^{-1} at 4.2 K, and is large enough so that the mean temperature of the sample does not vary by more than ~ 0.05 K while the field is swept.

The recording procedure just described is also used to determine the critical field at the current temperature. The magnetic field is then adjusted to that critical value, and the thermal conductivity is measured. The critical-field conductivity is needed to calculate the intermediate-state conductivity from the recorded trace. In this calculation, the calibration curves of the thermometers are assumed to be locally exponential, which is an excellent approximation. The same procedure is used to record and calculate the field variations of the thermal conductivity above the critical value.

The magnetic field is applied obliquely, with a large component in the direction of the heat current (Section 4). It is produced by a pair of Helmholtz coils, and this, together with the avoidance of magnetic or superconducting materials, as well as all brass,‡ ensures a field homogeneity of 0.6% along the sample between the main thermometers.

*See Section 5. The period a and the concentration x_N change along the sample since the value of the critical field depends on the local temperature.

†In this way, diffusion of impurities into the sample—which might have occurred if the latter had been soldered to the holder—is avoided.

‡Several brasses contain lead, and their magnetization curve has the character of that of a superconductor, as was verified in our laboratory.

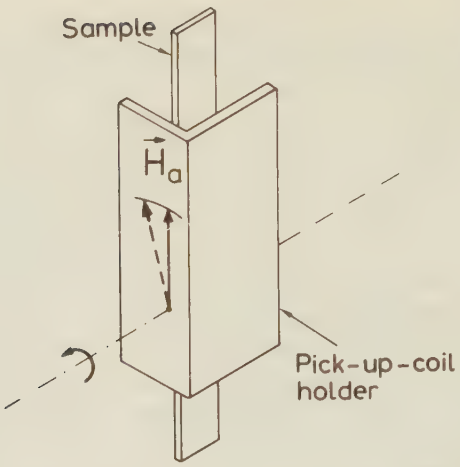

Fig. 4. Adjustment of the angle between the sample and the applied magnetic field $\mathbf{H}_a$. Two small, flat pickup coils perpendicular to one another are wound around the edges of the corner, which is screwed on the sample holder, parallel to the sample. The Helmholtz coils producing the field are moved until the voltage surges induced in the pickup coils by switching on and off the field disappear. Then the Helmholtz coils are rotated by the desired angle around the indicated axis.

Consequently, according to the results of Section 4, the period of the intermediate-state structure varies by 10% and the N phase concentration by 9%, in the worst case, along the same distance.

The angle between the field and the heat current, at large distances from the sample, is usually 15°. This angle is one of the parameters determining the intermediate-state structure, and is controlled in the following way, before filling the cryostat with liquid helium. The field is first set parallel to the long edges of the sample; then the Helmholtz coils are rotated by 15° around a horizontal axis parallel to the sample. The parallelism is controlled by measuring the voltage induced in two perpendicular pickup coils (Fig. 4) by switching on and off the current in the Helmholtz coils. Both pickup coils have been wound on a holder mounted parallel to the sample. The accuracy of this orientation adjustment procedure is $\frac{1}{2}°$.

4. LONGITUDINAL LAMELLAR STRUCTURES

In a preliminary study we determined several properties of the selected intermediate-state configuration, the longitudinal lamellar structure

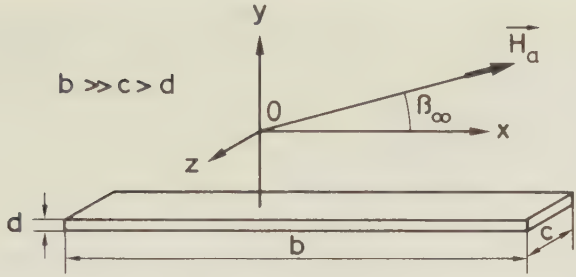

Fig. 5. Sample and magnetic field geometry. Following Sharvin,[9] the field is applied obliquely. The longitudinal lamellar structure is observed only in a particular field range in decreasing the field from the critical value $H_c(T)$ (N–I transitions). See text.

(LLS).* First of all, we studied by direct observation the conditions required to obtain such structures. The period of the LLS was then determined optically in both lead and tin. Finally, the concentration x_N of the N phase in the LLS was deduced from thermal conductivity measurements on the impure sample Sn 2.

As first observed by Sharvin,[9] the magnetic field, when applied obliquely (Fig. 5), has an aligning effect on the intermediate-state structure in a plate. This effect, however, is observed only if the applied field is not too far below the critical value. The reason is that the field *inside* the plate has a component in the direction of the plate axis which becomes smaller and smaller as the applied field is reduced. This can be easily understood in substituting for our sample an ellipsoid and writing the relations between the applied field $\mathbf{H}_a$ and the fields $\mathbf{B}$ and $\mathbf{H}$ inside the sample[38]:

$$H_i = H_{ai} - D_i M_i, \qquad B_i = \mu_0(H_i + M_i) = \mu_0 x_N H_i \qquad (i = x, y, z) \quad (8)$$

with $|\mathbf{H}| = H_c(T)$ and $\sum D_i = 1$. Here $\mathbf{M}$ is the magnetization, and D_i the three demagnetizing coefficients of the sample. x_N is the concentration of the N phase. Due to the particular choice of the plate shape and of the axis (Fig. 5), one has $D_x \approx 0$, $D \equiv D_y > D_z$. Hence

$$\operatorname{tg} \beta = [1 - D(1 - x_N)]^{-1} \operatorname{tg} \beta_\infty \quad (9)$$

where β is the angle of $\mathbf{H}$ with the plate axis inside the plate, and β_∞ the angle between the applied field and the plate axis, at large distances (Fig. 5). For constant β_∞, β increases from β_∞ to nearly 90° (since $D \approx 1$) as x_N decreases from 1 to 0.

For simplicity, the whole study of the intermediate-state thermal conductivity has been made with one single value of β_∞. The value chosen, 15°, is a compromise: For larger values, the aligning effect is reduced, while

*The concept has been defined in the introduction. See Fig. 1.

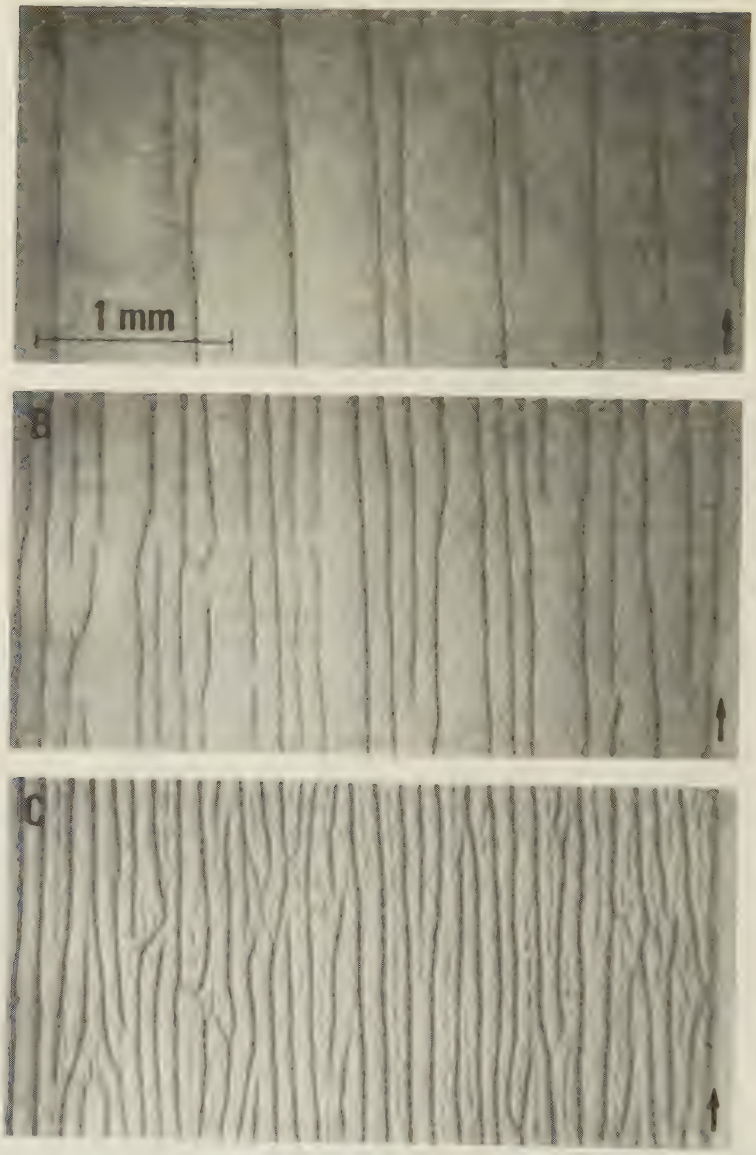

Fig. 6. Intermediate-state structures successively observed in decreasing the applied field from the critical value $H_c(T)$. Here $T = 4.25$ K, $\beta_n = 15°$. Values of the reduced field $h = H_a/H_c(T)$: (A) 0.988; (B) 0.967; (C) 0.923; (D) 0.868; (E) 0.753; (F) 0.642; the field was decreased to zero and inverted between E and F. The same part of the sample is seen on all the photographs, the arrow indicates one sample edge. The pictures were taken using a high-resolution magnetooptical technique, the sample and field geometry being the same as during the thermal conductivity measurements (see Fig. 5).

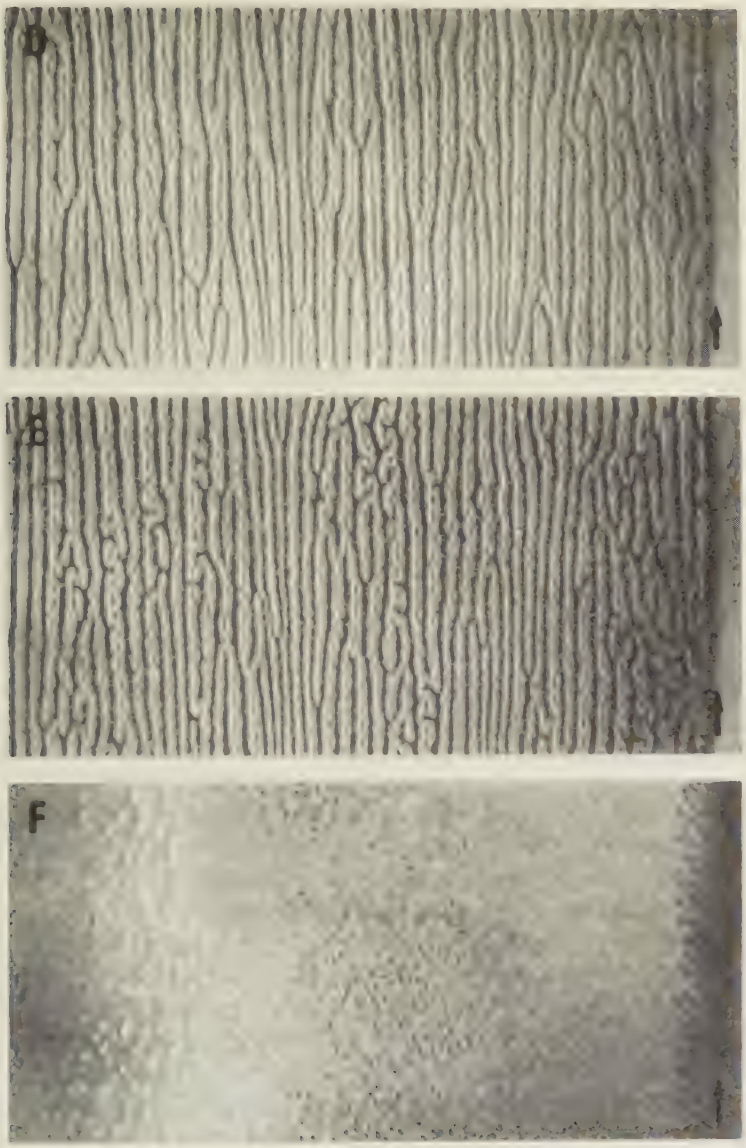

Fig. 6. Continued. (A–E) The superconducting domains are dark. The first superconducting lamella is shifted with respect to the sample edge, probably because the edge is not completely sharp in the neighborhood of the magnetooptical layer. (F) The light regions are "frozen-in" flux in the center of the sample; the dark ones are flux tubes of the opposite sign issued from the edge region where partial flux penetration occurs; the remainder of the sample is in the superconducting state.

for smaller values the concentration x_N varies too quickly with the applied field near the critical value (see below). Furthermore, to avoid having to determine the structure characteristics for each sample, all samples were of approximately the same size (i.e., the same D).

Before the thermal measurements we studied the formation of the LLS, using a high-resolution magnetooptical technique. The sample used for this study was a polycrystalline, high-purity lead plate, from the same ingot as Pb 1. Its size ($50 \times 5 \times 0.55$ mm^3) was chosen to give nearly the same demagnetizing factor D as for the samples used for the thermal measurements. The central part of the plate was observed, including the two edges. β_∞ was mechanically adjusted to $15° \pm \frac{1}{2}°$.

Our observations indicate that the different topologies observed by Haenssler and Rinderer[11] in a plate placed perpendicular to the field are also present when the field is oblique. In the structures obtained by S–I transitions [field increased from 0 to $H_a < H_c(T)$], the N domains are flux tubes surrounded by a S matrix, except near the plate edges, where reversible partial penetration takes place; flux penetration into the bulk sample does not occur below a certain threshold value of the field.[39] It is concluded that S–I transitions are not suitable to create the LLS, except in a very small field range just below $H_c(T)$.

On the contrary, N–I transitions [field decreased from above $H_c(T)$ down to $H_a < H_c(T)$] produce the LLS, provided the field is varied slowly enough. The growth and evolution of the LLS is as follows.* Just below $H_c(T)$, a S lamella is observed suddenly, coming from one plate end and growing in the direction of the plate axis. Later, many such lamellas grow parallel to the first one (Fig. 6A). On further reduction of the field, certain lamellas become locally thicker and bend slightly; then, suddenly, a new S lamella grows from this point, parallel to the other lamellas (Fig. 6B). Some "bridges" between two S lamellas are also observed. For $h = H_a/H_c(T) \lesssim 0.95$, short S lamellas appear in the middle of the N lamellas (Fig. 6C); they probably do not extend over the whole thickness of the plate ("branching"). At the same time, flux expulsion begins at preferred points along the plate edges. The S lamellas move to these points and break up there. On continuing with field reduction, one observes more complicated structures (Fig. 6D); the "branching" becomes more important, and the width of the two edge regions with irregular lamella arrangements increases. For $h \lesssim 0.85$, some central N lamellas become corrugated due to alternating "dendritic" side growths of the two adjacent S lamellas; the aligning effect of the field disappears progressively (Fig. 6E). For $h \lesssim 0.65$, only some N

*Our description of the growth process differs slightly from that given by Farrell *et al.*[40] This can be due to not quite identical geometrical conditions (sample size, value of β_∞).

TABLE II

Imperfections Observed in the LLS Obtained by N–I Transitions with $\beta_\infty = 15°$ [a]

Imperfection	Reduced field h	
	0.90	0.75
Edge effect, % of sample width	5	10
Length of S or N lamella between two successive splittings, mm	7.5	6.6
Number of corrugated lamellas, % of total number of lamellas	—	10 [b]

[a] Sample thickness 0.55 mm.
[b] Corrugations are observed only on half the length of a lamella.

lamellas are still straight. Then, lateral flux expulsion goes on in the form of serpentins and is discontinuous. When the field is zero, a certain amount of "frozen-in" flux still remains; these tubes are not expelled before the penetration of the flux tubes of the opposite sign, which occurs in increasing the field after inversion (Fig. 6F).

It is concluded that, for $\beta_\infty = 15°$, N–I transitions with $0.7 \lesssim h \lesssim 0.98$ can be used to create LLS approaching the ideal one of Fig. 1. The number and type of defects observed at two different field values are listed in Table II. As will be seen, these defects have only little influence on the thermal conductivity of the whole structure.

The period a of the LLS obtained by N–I transitions with $\beta_\infty = 15°$ was determined independently for lead and tin. For lead we used the sample and technique just described. The period was measured on photographs, the plate width being used as reference length. The values quoted on Fig. 7 were averaged over the whole plate width, excluding, however, the two disturbed regions near the edges. Internal subdivisions of a N lamella, such as, for example, "branching" or corrugation, have been ignored. The error bars on the graph indicate the counting error. The critical field $H_c(T)$ was determined optically; it is the mean of two values differing generally by 0.5%; the first corresponds to the disappearance of the last S domain in S–I transitions, and the second to the appearance of the first S lamella in N–I transitions. The mean temperature was then calculated from $H_c(T)$.[41]

For tin, the measurements of the structure period were made when the magnetooptical apparatus was not yet available; we used the diamagnetic (Nb) powder method[42] to reveal the structure; a was calculated from the photographs as for lead. In order to check the thickness dependence of a, we prepared three plates of different size (see Table III). As can be seen on

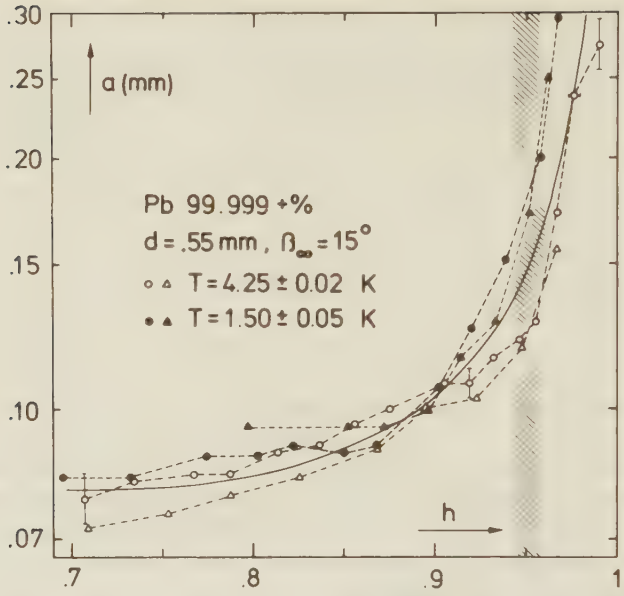

Fig. 7. Period of the LLS in the case of lead, as measured on photographs taken using a magnetooptical technique. The symbols refer to four different N–I transitions. $h = H_a/H_c(T)$. For $h \gtrsim 0.95$, the total number of lamellas increases as h is reduced; the apparent temperature dependence of the period is not significant. For $h \lesssim 0.95$, the period decreases irregularly, as a consequence of the action of the pinning forces, which prevent the interphase boundaries from moving freely to the sample edges. The solid curve is calculated from the Landau–Sharvin theory, with adjustment of the surface energy parameter to give the experimental value of a at $h = 0.9$. See text.

TABLE III

Tin Samples Used in the Determination of the Period of the LLS

	Size, mm		
Sample[a]	*b*	*c*	*d*
Sn 9	50	10.05 ± 0.15	0.915 ± 0.005
Sn 7	50	19 ± 1	0.753 ± 0.003
Sn 3	50	19 ± 1	0.302 ± 0.004

[a] Supplier: Vulcan Detinning. Purity: 99.9999%.

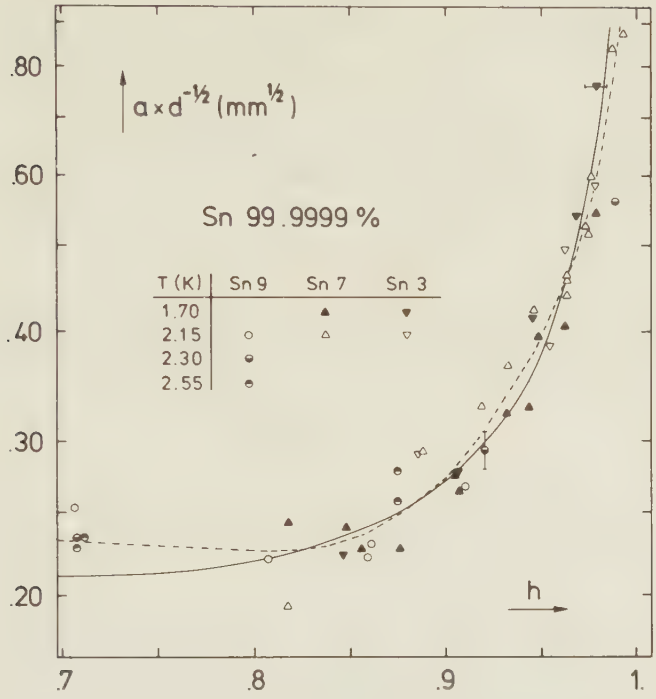

Fig. 8. Period of the LLS in the case of tin, as measured on photographs taken using the Nb-powder method to reveal the structure, in three samples of different thicknesses d. N–I transitions; $\beta_\infty = 15°$; $h = H_a/H_c(T)$. The vertical axis has been rescaled for each sample according to its thickness to show the invariance of $ad^{-1/2}$. The temperature dependence is not significant. The dashed line is the mean value introduced into the theoretical expressions of the size effect (Section 5.3). The solid curve is calculated from the Landau–Sharvin theory with adjustment of the surface energy parameter. See text.

Fig. 8, $a \propto d^{1/2}$ within the experimental errors. The latter are more important than for lead, due to the different observation technique and the occurrence of supercooling in tin. The critical field cannot be determined as accurately as for lead. Furthermore, the diamagnetic powder must be removed after each photograph is taken, in order to avoid subsequent disturbance of the intermediate-state structure. Finally, the angle β_∞, which had to be readjusted after removing the powder, was reproducible to only $\pm 1°$.

The concentration x_N of the N phase in the LLS was determined by thermal conductivity measurements on Sn 2. This tin sample is impure

enough so that the electronic mfp ($=1.3\mu$m)* is much smaller than the structure period. Consequently, impurity scattering is much more important in the intermediate state than interphase boundary scattering. (i) The quasiparticles cannot cross a lamella without being scattered by an impurity, and the trapping mechanism involved in Andreev's size effect[17] cannot take place. (ii) The structure defects (see Table II), which will be seen to have only a small influence on the conductivity when the sample is pure (see Section 5), modify even less the conductivity in the impure sample.†

Thus, in Sn 2, the concentration x_N in the LLS can be determined from Eq. (7), where K, K_N, and K_S are the measured thermal conductivity in the intermediate, normal, and superconducting states, respectively. One gets

$$x_N = \left(1 + \frac{w}{(1-w)f(T)}\right)^{-1}$$

The quantity $w = (W - W_N)/(W_S - W_N)$ can be easily obtained from the recorded traces. Here $f(T) = W_N/W_S$, and W, W_N and W_S are the thermal resistivity in the intermediate, normal, and superconducting states, respectively.

The results are displayed in Fig. 9 and Table IV. The uncertainty (indicated in the table) is mainly due to the poor definition of H_c on the recorded traces (see Fig. 11), and to the uncertainty in W_S due to frozen-in flux (only, however, for the lower x_N values).

Our experimental results on the period a and the concentration x_N of the LLS will now be compared to the predictions of the well-known intermediate-state model of Landau,[30] which was extended by Sharvin to the case of an oblique magnetic field[9] [the Landau–Sharvin (LS) theory‡]. The period and the concentration given by the LS theory are

$$a^{LS} = [\Delta d/\phi(x_N)]^{1/2}(1 - h^2\cos^2\beta_\infty)^{-1/2} \tag{10a}$$

and

$$x_N^{LS} = h(\sin\beta_\infty)(1 - h^2\cos^2\beta_\infty)^{-1/2} \tag{10b}$$

Here, Δ denotes the surface energy parameter and $\phi(x_N)$ a dimensionless function tabulated by Lifshitz and Sharvin.[46] It is emphasized that the LS theory assumes the plate to be infinite in two directions and much thicker

*Deduced from the residual resistivity ρ_0 and the value $\rho_0 l = 1.05 \times 10^{-11}\ \Omega\,\text{cm}^2$ obtained from the anomalous skin effect.[43]

†The temperature jump per heat current density at an N–S interphase boundary was shown to be only weakly purity dependent in tin (see Ref. 18).

‡A detailed description of the LS theory is given in Ref. 44. For further comments, see also Ref. 45.

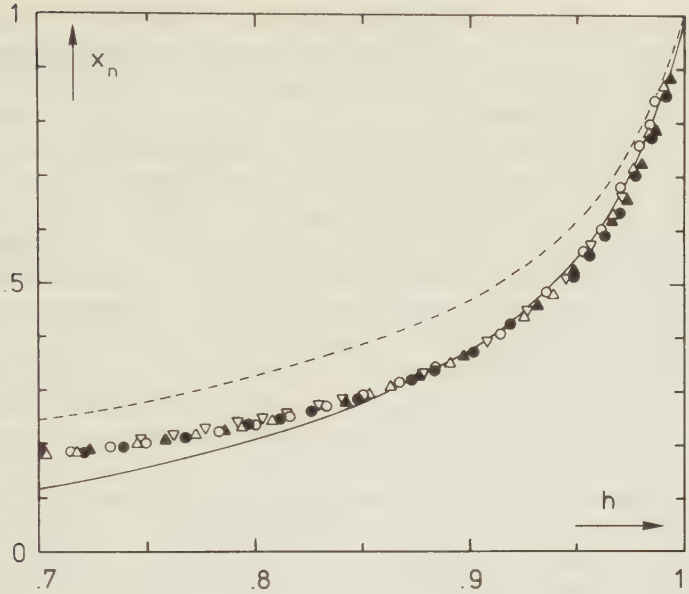

Fig. 9. Concentration of the normal phase of the LLS vs. the reduced applied field $h = H_a/H_c(T)$. N–I transitions; $\beta_\infty = 15°$. x_N is calculated from thermal conductivity data on the "impure" sample Sn 2 (see, e.g., part D–E of the curve of Fig. 11). Sample and field geometry are the same as in the study of the size effect. The symbols refer to five different thermal resistivity curves at constant temperature: (○, △, ▲) 1.7 K; (●) 1.8 K; (▽) 1.9 K. The dashed curve is calculated from the Landau–Sharvin theory, Eq. (10b), and the solid curve from its extension to finite sample size, Eq. (11), with $D = 0.85$. See text.

TABLE IV

Concentration x_N of the N Phase in the LLS (N–I Transitions, $\beta_\infty = 15°$) vs. the Reduced Applied Field h[a]

h	x_N	h	x_N
0.612	0.144	0.919	0.420
0.749	0.200 ± 0.006	0.935	0.470
0.783	0.225	0.953	0.545
0.813	0.250	0.961	0.590
0.851	0.290	0.973	0.675 ± 0.03
0.867	0.313	0.983	0.770
0.884	0.340	0.987	0.820
0.901	0.374	1.	1.

[a] From the experimental data of Fig. 9. The quoted values were chosen in such a way that linear interpolation between them is possible within the experimental error on x_N.

than the period. These conditions are, however, only approached in our case (Table I; Figs. 7 and 8). Thus, one should not expect too good an agreement between theory and experiment.

The period calculated from Eq. (10a) is given in Figs. 7 and 8. The surface energy parameter was adjusted to give the observed value of a at $h = 0.9$. In the temperature ranges studied, we obtain $\Delta = 1.06 \times 10^{-5}$ cm for Pb and 4.05×10^{-5} cm for tin. The published values of Δ are spread over large intervals ($\sim 300\%$ variation for each metal)*; our values lie among the largest quoted, for both lead and tin. As can be seen from Figs. 7 and 8, the calculated h dependence of a is roughly in agreement with the observed one. However, the comparison cannot be pushed further, due to the large scatter of the data points. In particular, as already noted by Sharvin,[9] it does not make sense to study the possible (small) influence of the finite size of the samples, although this influence ought to be larger than in the disks studied by Sharvin.†

The situation is different for the concentration x_N, for which accurate data are available (Fig. 9; Table IV). Equation (10b), which does not contain any adjustable parameter, gives a result that deviates systematically from the experimental data (Fig. 9). Going back to Eq. (8) to account for the finite size of the plate, one obtains easily

$$x_N = x_N^{LS}/D - (1-D)/D \tag{11}$$

which generalizes Eq. (10b) to $D \neq 1$. The calculated x_N is now found to agree with the observed data by adjusting the principal demagnetizing coefficient D to 0.85 (Fig. 9). The latter value is a reasonable one for our plates, for which the inscribed ellipsoid has a principal demagnetizing coefficient of 0.91.[49] The deviation between the calculated and the observed concentrations below $h \approx 0.85$ can be explained by delayed flux expulsion due to sample defects.

For the interpretation of the thermal conductivity data (next section), our *experimental* data on a and x_N will be used systematically [however, not in Fig. 13 and in evaluating Eq. (12)].

5. THE SIZE EFFECT

5.1. Existence of a Nontrivial Effect

To see that the conductivity of the LLS in a pure sample differs fundamentally from that of the LLS in an impure sample is not straightforward. This is due to the fact that, in the recorded variations of the

*For a review of the published data on Δ, see Ref. 47 for Pb and Ref. 48 for Sn.

†The principal demagnetizing coefficient of our samples is mainly determined by the ratio thickness/width $\approx 1/10$.[49] The ratio thickness/diameter of Sharvin's disks was 1/25.[9]

thermal resistivity, the most striking difference between a pure (Fig. 10) and an impure (Fig. 11) sample is the presence of a peak in increasing the field in a pure sample. This peak was already observed in early work on cylindrical samples.[1–5] However, if one remembers that the intermediate-state structure here consists of flux tubes, it is immediately seen that the peak is due to the electronic transverse thermal resistance of the interphase boundaries and/or to the phonon-mfp reduction in the S domains (see the introduction)! The temperature dependence of the height of the peak is in qualitative agreement with previous work (see, for example, Ref. 3), but a simple calculation of the peak shape taking into account geometrical aspects of the complicated intermediate-state structure is not possible. The same applies to the smooth maximum observed at $h \approx 0.4$ in decreasing field.

According to Section 4, the LLS exists between points D and E of the recorded traces. But no significant difference between the pure sample and the impure one can be noted on these parts of the curves. The difference becomes evident only when the thermal *conductivity* is calculated (see below, Fig. 15). At this point of the analysis, it is seen that unambiguous identification of the experimental data to be analyzed in the search for Andreev's size effect would have been impossible without the direct observation of the intermediate-state structure reported in Section 4.

We now demonstrate that the heat current, which is maintained through the sample when the field is swept, does not influence the measured resistivity (Fig. 12). The same resistivity cycle was described twice. The first time, the heat current was permanently on (cycle "$Q \neq 0$"). The second time it was switched on only to allow the measurement of the thermal resistivity, at more or less regular intervals. As can be seen, the resistivities are practically identical.

The small residual deviations are nearly always observed (see also Fig. 10), and are not reproducible; the faster the field is swept, the larger are the deviations. The sweep time, however, cannot be increased beyond 10–20 min, as otherwise the thermal voltage drift in the measuring bridge becomes too important.

These residual deviations in the resistivity are thought to originate in the nonreproducibility of the intermediate-state structure due to sample defects. (i) Their amplitude is maximum in decreasing field for $h \lesssim 0.5$, where impulsive flux expulsion occurs. (ii) After a sudden small field change, the time required by the recorder pen to reach the previously quasistatically recorded trace is comparable with the time during which interphase boundary displacements were observed (with the magneto-optical technique) after a similar field change.

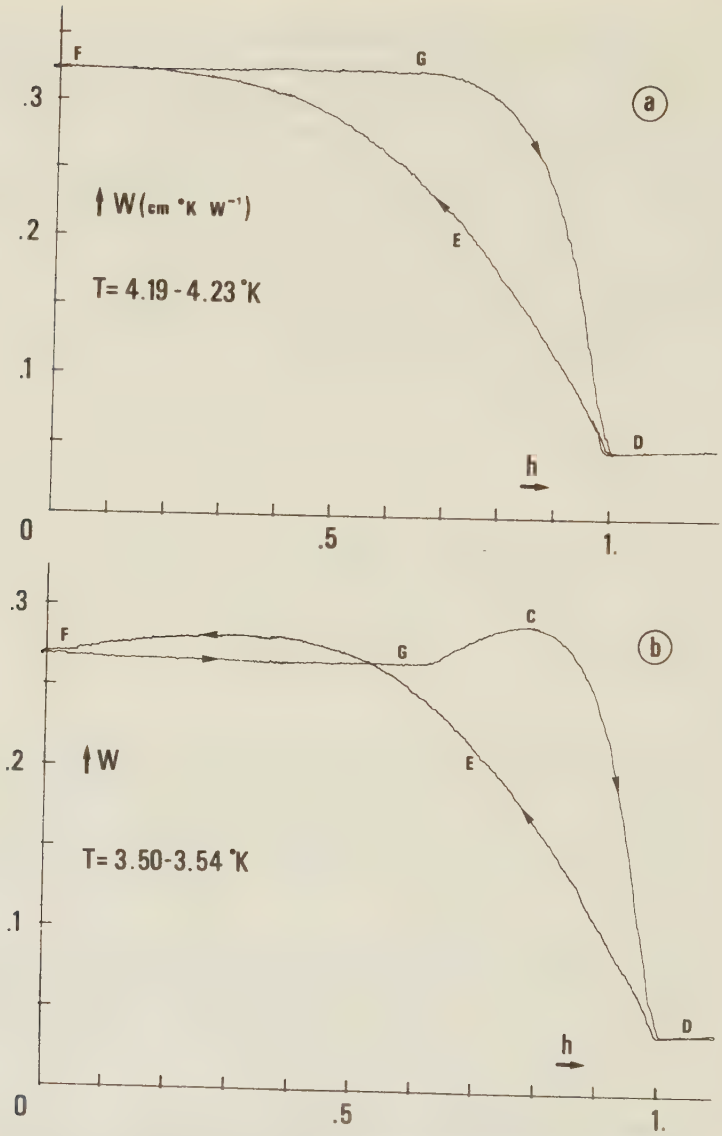

Fig. 10. Thermal resistivity cycles recorded at different temperatures with the pure sample Pb 1. (A) Superconducting state without "frozen-in" flux. (B) First flux penetration into the bulk of the sample. (C) The sample contains a maximum number of flux tubes. (D) Normal state. (D–E) Range of existence of the LLS. (F) The field is inverted. (G) Penetration of new flux into the sample. Like the intermediate-state structure itself, the recorded curves are not exactly reproducible. The two, strongly temperature-dependent peaks at $h \approx 0.8$ and $h \approx 0.4$ correspond to complicated structures and cannot be interpreted quantitatively in a simple way. In the present study, we restrict ourselves to the part D–E of the curves. The mean temperature of the sample varies during a cycle between the two values indicated.

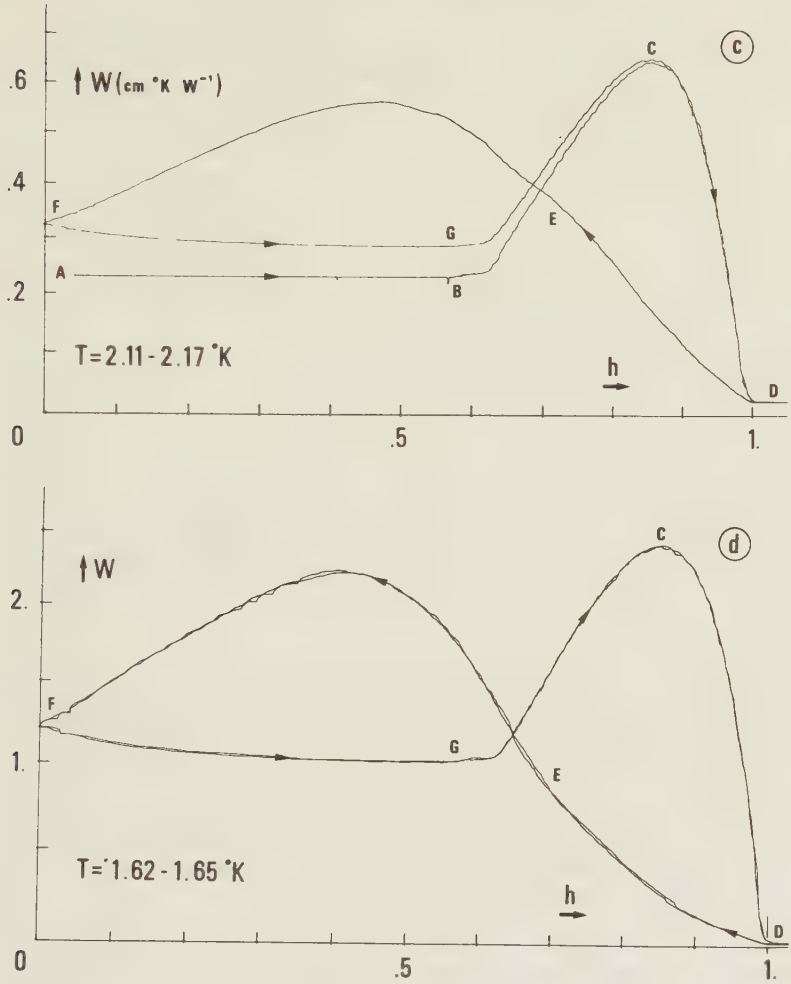

Fig. 10. Continued.

In deducing the presence of Andreev's size effect in the LLS, we require an expression for the thermal conductivity that may be theoretically expected in the LLS without the size effect. The following expression is convenient:

$$K(T, x_N) = x_N K_N[T, H_c(T)] + (1 - x_N) K_S(T) \tag{12}$$

Equation (12), which is formally equivalent to Eq. (7) (short-mfp limit), takes into account the field dependence of the conductivity in the N phase, but neglects any quasiparticle exchange between lamellas of different kind.

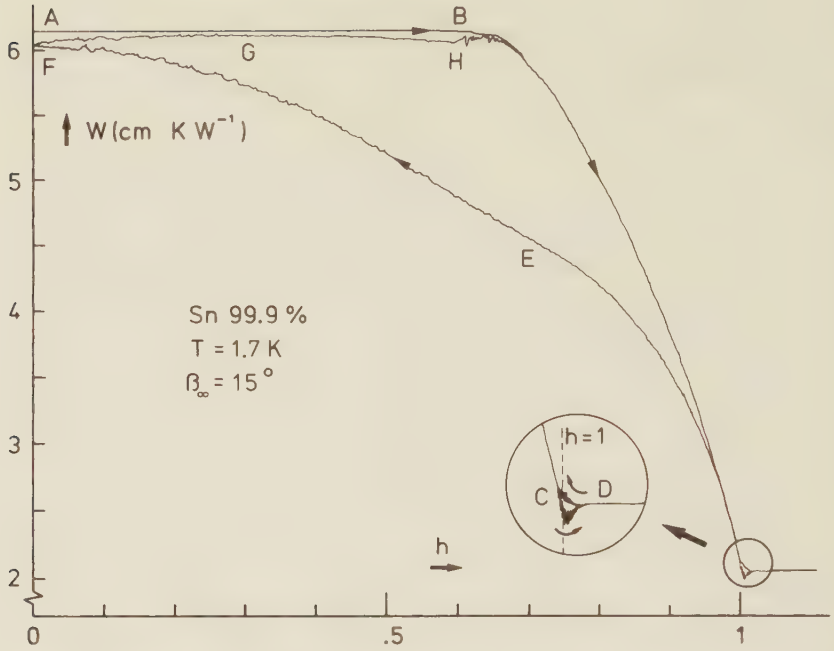

Fig. 11. A typical thermal resistivity cycle recorded with an "impure" sample (Sn 2). (A) Superconducting state without "frozen-in" flux. (B) First flux penetration into the bulk of the sample. (C) The last S domains disappear. (D) First nucleation of S lamellas. (D–E) Range of existence of the LLS. (F) The field is inverted. (G) Resistivity maximum (however, lower than in the pure S state because of "frozen-in" flux). (H) Expulsion of the last "frozen-in" flux and penetration of new flux (see Fig. 6F). The sharp, transient temperature peaks observed in C, D, and H correspond to release or absorption of latent heat due to sudden phase transition in large parts of the sample. These peaks cannot be observed in the pure samples.

The corresponding plots will be denoted by the mnemotechnic notation MR,–, indicating that the magnetoresistance is taken into account in the N phase, while Andreev's size effect is neglected in the S phase.

As noted in Section 4, Eq. (9), the angle β between the field $\mathbf{H}$ and the plate axis, i.e., the heat current $\mathbf{q}$, depends, in a N lamella, on the concentration x_N. Thus, the angular dependence of $K_N[T, H_c(T)]$ is needed in evaluating Eq. (12). This can be obtained from the most general linear relation between the temperature gradient and $\mathbf{q}$:

$$-\nabla \mathbf{T} = a\mathbf{q} + b\mathbf{n} \wedge \mathbf{q} + c\mathbf{n}(\mathbf{n} \cdot \mathbf{q})$$

Here $\mathbf{n}$ is a unit vector in the direction of $\mathbf{H}$, and a, b and c are scalar quantities depending on $|\mathbf{H}|$. By projection onto the plate axis (denoted by

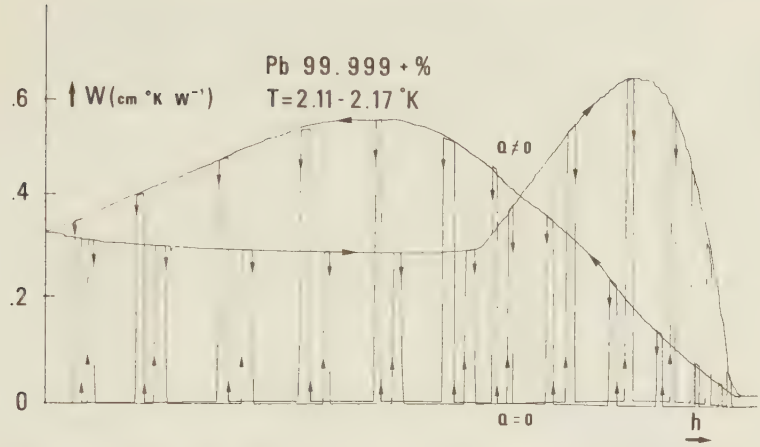

Fig. 12. Validity check of the constant-heat-flow measuring procedure used for the recording of the intermediate-state thermal resistivity. The same resistivity cycle has been described twice. (1) $Q \neq 0$: With a constant heat current during field sweep. (2) $Q = 0$: The heat current is switched on only to allow thermal resistivity measurements. The measured resistivity is the same in both cases. See text.

x), we find the desired β dependence of the thermal resistivity (the measured quantity)

$$W_\beta \equiv W_{xx} = -\partial_x T/q = a + c\cos^2\beta$$

which can be more conveniently written as

$$W_\beta = W_0 + (W_{90} - W_0)\sin^2\beta \tag{13}$$

where W_0 and W_{90} are the longitudinal and transverse resistivities, respectively, at particular values of $|\mathbf{H}|$ and T. A rough check of Eq. (13) is shown in Fig. 13; the $\sin^2\beta$ dependence is verified in the first approximation. Also shown (lowest horizontal scale) is the concentration x_N of the N phase in the LLS for $\beta_\infty = 15°$ vs. β; it was calculated from Eq. (9) with $D = 0.85$.* In the x_N range where the LLSs have been shown to exist and are sufficiently free of defects ($0.2 \lesssim x_N \lesssim 0.7$), β varies from 20° to 40°, and Eq. (13) is followed to within 10%, which is sufficient for the purposes of our analysis.

We are now going to show that there exists, in pure samples; a nontrivial thermal conductivity reduction in the LLS. Sample Pb 1 was chosen for this purpose, but the same developments could have been made for Sn 1 without lack of generality.

*This value of D gives the best fit of the curve $x_N(h)$ if delayed flux expulsion below $h \approx 0.85$, i.e., for $x_N \lesssim 0.3$, is neglected (see Fig. 9).

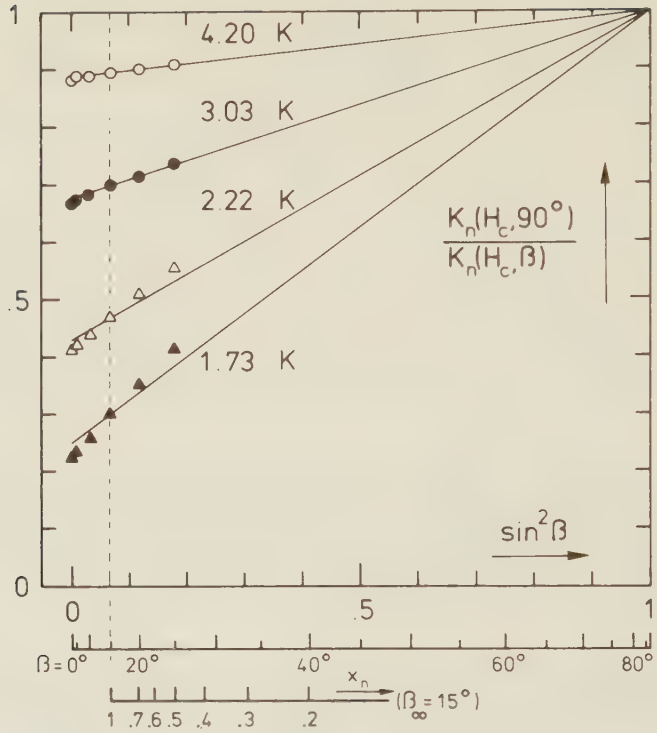

Fig. 13. Thermal resistivity of Pb 1 in a critical field at four temperatures as a function of the angle β between field and heat current. The results are normalized with respect to the transverse-field resistivity at the current temperature. The straight lines are drawn through the two most accurate data-point sets, those corresponding to $\beta = 15°$ and 90°. The linear $\sin^2\beta$ dependence is followed in the first approximation [Eq. (13)]. The lowest horizontal scale gives, for a given β, the corresponding value of the N-phase concentration in the intermediate state when the angle β_∞ between field and heat current *at large distances from the sample* is 15°. See text.

We first go on with the determination of the quantities entering Eq. (12). Figure 14 gives the temperature dependence of the conductivity of the S and N phases, the latter for five H and β_∞ values.* The large field anisotropy of K_N, especially at lower temperatures, is to be noted (see also Fig. 13). Although the field is not larger than ~ 1 kOe, the magnetoresistance is important in our high-purity sample. However, the conductivity reduction in the S phase below T_c is more important, as a direct consequence of the strong coupling character of lead. Thus, $K_S(T)$ is

*The extrapolation procedure used to obtain the curve N_0 is given in Section 5.2.

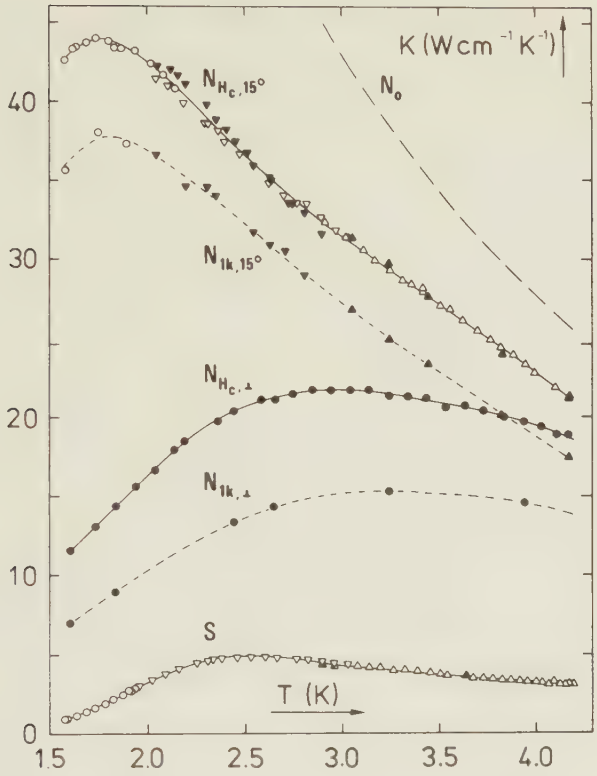

Fig. 14. Thermal conductivity of Pb 1. Here S denotes the frozen-flux free, superconducting state, and N the normal state (five curves); the first index indicates the applied-field value [$H_c(T)$ or 1.03 kOe], and the second index the angle between the field and the heat current (15° or 90°). N_0 is the zero-field extrapolated, normal-state conductivity. The data points are represented by different symbols to distinguish between the successive thermometer calibrations used for the calculation of K. The thermometers were recalibrated after each warming up to room temperature.

smaller (at lower temperatures, much smaller) than $K_N[T, H_c(T)]$. This important feature will be used in the next section.

In Figs. 13 and 14, the conductivity K_N was calculated by taking the reciprocal of the measured resistivity. Thus, the Righi-Leduc effect has been neglected. The error introduced by the procedure is equal to $\mathrm{tg}^2\theta_{RL}$, θ_{RL} being the thermal analog of the Hall angle θ_H. No data could be found on the Righi-Leduc effect in lead, so that we estimated the error from data on the Hall angle at $H = H_c(T)$ obtained optically in our laboratory[41] using

the orienting effect of an electrical current on the intermediate-state structure.[50] Lead is a compensated metal, and $\theta_H[H_c(T)] \approx 10°$, typically, in a perpendicular field. Since the field is oblique in our case, its transverse component, which determines the effect, is $H_c(T) \sin \beta$, with $\sin \beta = 0.35$–0.65, depending on the value of x_N. Thus, the Hall angle is also reduced, say, by a factor $\sin \beta$. Finally then, the error $\mathrm{tg}^2 \theta_{RL}$, is about 1–2%, and can be neglected compared to the experimental error in K.

The N-state thermal conductivity in a critical field $K_N[T, H_c(T)]$ was not measured for each value of β and T. In evaluating Eq. (12), we used the data of Fig. 14 for $\beta = 15°$ and $\beta = 90°$. For a given x_N, the value of β is calculated from Eq. (9) with $D = 0.85$; then, $K_N[T, H_c(T)]$ is obtained from the $\sin^2 \beta$ dependence of the resistivity [Eq. (13)]. Let us mention for completeness that the value of K_N calculated in this way is assumed to be valid for the whole sample. Longitudinal concentration gradients (Section 3.2) are thus ignored, and the calculated K_N is some average of the actual K_N.*

In Fig. 15, the thermal conductivity of the LLS, calculated with Eq. (12), is compared to the experimental data. It is seen that the curve MR,−[Eq. (12)] differs essentially from the data points. Similar results are obtained at other temperatures. It is concluded that the magnetoresistance in the N lamellas is not sufficient to explain the reduction in the thermal conductivity observed in the LLS.

This conclusion is even reinforced if the variation of the mean critical field in the sample during the recording of a resistivity cycle is taken into account, unlike in Fig. 15. When the applied field is decreased from the critical value, the mean temperature of the sample is slightly increased (up to ~ 0.03 K in the range of existence of the LLS; see Fig. 10). Consequently, the reduced field $h = H_a/H_c(T)$, and hence the concentration x_N, have been underestimated in our calculation. The deviation amounts to 10% in the worst case ($T = 4.2$ K, $x_N = 0.7$).

Also shown on Fig. 15 is K_0, the theoretically expected thermal conductivity without magnetoresistance and size effect:

$$K_0(T, x_N) = x_N K_N(T, H = 0) + (1 - x_N) K_S(T) \tag{14}$$

where $K_N(T, H = 0)$ is the N-state conductivity extrapolated to zero field (see Section 5.2). The quantity K_0 is interesting because its x_N dependence is trivial, and it will be used to normalize our results so that the effects studied are more clearly delineated.

*At a given value of the applied field, the longitudinal variation of K_N is small since x_N changes along the sample by less than 10% in the worst case. This is because the temperature range studied is far enough below the critical temperature of lead.

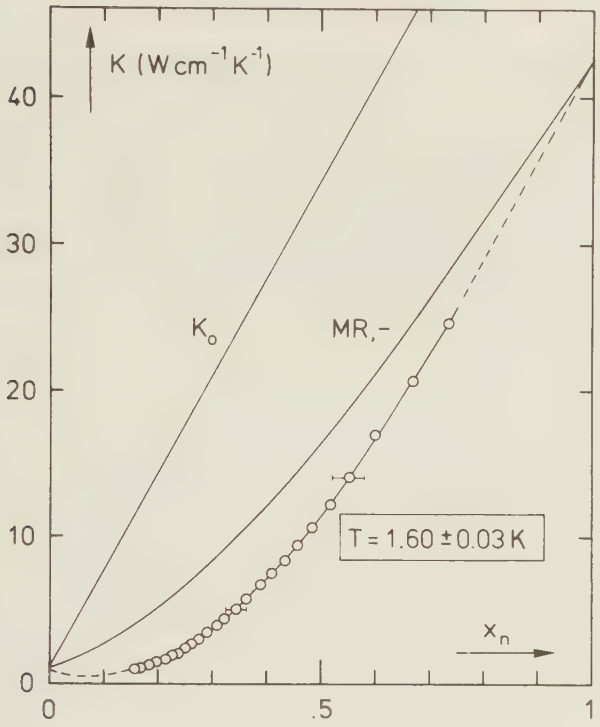

Fig. 15. Typical thermal conductivity curve of the LLS in Pb 1 (data points) vs. the concentration of the N phase. The observed thermal conductivity reduction cannot be explained by the simple model of Eq. (12) (curve MR,–), which takes into account the thermal magnetoresistance in the N lamellas. K_0 is the theoretically expected thermal conductivity without magnetoresistance and size effect [Eq. (14)]. The error in T indicates the increase in the mean temperature of the sample when x_N is reduced via the applied field. For $x_N \lesssim 0.2$ and $x_N \gtrsim 0.7$, other intermediate-state structures than LLS are observed (see Section 4).

The influence of the imperfections of the LLS have now to be considered (see Table II). (i) Edge effects or some corrugated lamellas do not affect in practice the measured conductivity, since it is averaged over a large number of lamellas, most of which conduct heat better than the disturbed regions. (ii) A split N lamella that interrupts a S lamella has also little effect on the conductivity, since heat conduction occurs mainly through the N lamellas. (iii) However, the opposite situation, namely a split S lamella interrupting a N lamella, must be considered rather more closely. At the end of the N lamella the quasiparticles have to cross two interphase

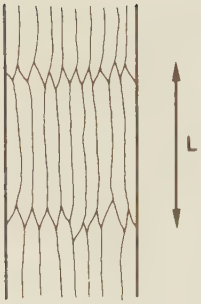

Fig. 16. Intermediate-state-structure model used in estimating the effect of the splitting of the S lamellas on the measured thermal conductivity of the LLS (Table V). The lines represent the S lamellas and the sample edges. The whole structure is periodic, and the period L is taken from Table II.

boundaries in order to get into the nearest, good conducting region. The additional thermal resistivity introduced by the boundaries may be estimated using the model shown in Fig. 16. All ramifications are assumed to be situated approximately on regularly spaced perpendiculars to the heat current, forming a set of large barriers across the whole plate. The distance between two consecutive barriers is taken from Table II. This model is of course unrealistic, but gives an *upper bound* of the disturbing effect of the ramifications. As can be seen from Table V, this effect is not important, although its exact value remains unknown. The observed reduction of the conductivity of the LLS in lead has therefore to be considered as nontrivial.

TABLE V

Additional Thermal Resistivity ΔW Introduced by the Splitting of the S Lamellas of the LLS, in Percent of the Measured Resistivity W[a]

		$\Delta W/W$, %	
T, K	W_{NS}, K cm^2/W	at $x_N = 0.375$, $h = 0.9$	at $x_N = 0.20$, $h = 0.75$
4.3	0.18×10^{-3}	0.4	0.25
2.3	2.15×10^{-3}	5	2

[a]The model of Fig. 16 is used to obtain an upper bound of the effect. The temperature jump per heat current density at the S–N interphase boundary W_{NS} was measured in our laboratory using a sample taken from the same ingot as Pb 1 (see Ref. 41).

5.2. The Size Effect in Lead

The intermediate-state thermal conductivity of Pb 1 for the case of the LLS is summarized on Fig. 17. To avoid the superposition of all the curves, the temperature T was chosen as the independent variable and the concentration x_N of the N phase as the parameter. The error on K (compared to Fig. 15) is thus increased by the experimental error in x_N. The scatter of the data points is larger than the random error,* since the intermediate-state thermal resistivity is not exactly reproducible (Section 5.1). The scatter of the data points is larger at lower temperatures,

*This random error arises essentially from the definition of the critical field on the recorded traces (see Fig. 10).

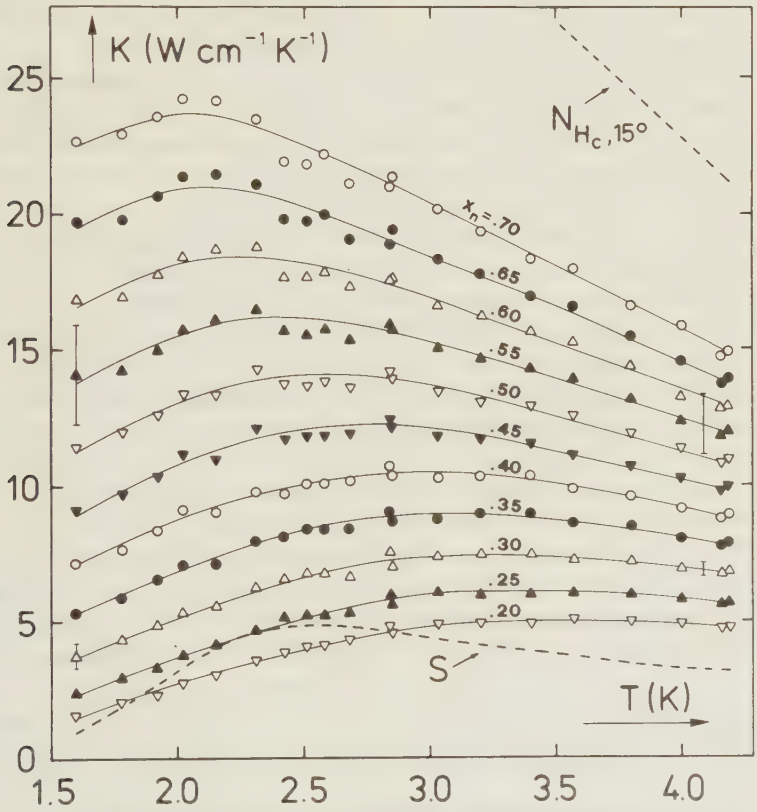

Fig. 17. Thermal conductivity of the LLS in Pb 1 at different temperatures and N-phase concentrations. The data are taken from 20 experimental curves like that of Fig. 15. The two dashed curves are reproduced from Fig. 14, for comparison. The experimental errors are discussed in the text.

corresponding to the well-known increased influence of the pinning centers. It is seen that the accuracy in the thermal conductivity measurements is satisfactory in comparison to the errors introduced by the intermediate state itself.

The results are analyzed at three different temperatures (Fig. 18). The conductivity has been normalized with respect to K_0, defined by Eq. (14). The departure of the data points from the MR,− curve appears clearly, as was already seen in Fig. 15. The two other theoretical curves* MR,SE and SE,SE are calculated from Eqs. (6) and (5), respectively, using the parameter values displayed in the lower part of each graph. It is seen that the principal parameter l_h/a_N can be varied by almost two orders of magnitude in the temperature and field ranges studied, using one single sample. a_N can be varied by one order of magnitude by varying the field, and l_h is decreased by a factor seven on going from 1.6 to 4.2 K. The latter fact is related to the low Debye temperature of lead.

The manner in which all the parameters are determined will now be discussed. (i) The width of the N and S lamellas is readily obtained from $a_N = x_N a$ and $a_S = (1 - x_N)a$, the period a being taken from Fig. 7 (after appropriate scaling according to $a \propto \sqrt{d}$). For lead the temperature dependence of a is neglected between 1.6 and 4.2 K.

(ii) The cyclotron radius in a critical field $r_c(T)$ is calculated by the free-electron model, with four electrons per atom, and the critical-field curve. At zero temperature, one obtains $r_c(0) = 0.135$ mm.

(iii) The mfp† l_h is determined from thermal and electrical conductivity measurements in overcritical magnetic fields. Extrapolation procedures to zero field are needed, which renders the determination of l_h more complicated and less accurate. However, no other possibility remains, since l_h has to be obtained in the same sample and under conditions approaching as much as possible those of Andreev's size effect. The detailed procedure consists in:

(a) Calculating the zero-field-extrapolated thermal resistivity in the N state from the curves $N_{1k,15°}$ and $N_{H_c,15°}$ of Fig. 14. Several extrapolation procedures have been attempted (quadratic, linear, etc.), the final values adopted being some average of all the results.‡ The T dependence of l_h is

*The mnemotechnic notations MR,SE and SE,SE indicate which phenomenon is taken into account in the N and S phases, respectively.

†We always use l_h to indicate the mfp of the heat carriers in the *normal* phase, even in the expression l_h/a_S.

‡The H dependence of the thermal resistivity has not been checked experimentally. As is seen from Fig. 18, $l_h/r_c \approx 1$ for $H_a = H_c(T)$, so that the low-field quadratic H dependence is probably not valid in our case. This assertion is also supported by the recent results of Higgins *et al.*,[51] who observed, immediately above the critical field, a deviation from the quadratic H dependence in the electrical resistivity of high-purity lead.

then readily obtained, as well as the residual electrical resistivity ρ_0 by the Wiedemann–Franz law.

(b) Measuring the electrical resistivity at different temperatures and then extrapolating it to zero field and zero temperature; the value of ρ_0 obtained in this way is averaged with that previously obtained.

(c) Calculating l_0, the impurity-limited mfp from $\rho_0 l_0 = 1.06 \times 10^{-11} \Omega\,\mathrm{cm}^2$ obtained by the anomalous skin effect.[43] The latter and Andreev's size effect have as common feature that the main role is played in both effects by electrons having a velocity nearly parallel to a certain plane. The final result is $l_0 = 0.3\ \mathrm{mm} \pm 30\%$, which, together with the T dependence of l_h, was used to recalculate the values of $K_N(T, H = 0)$ introduced into Eq. (5) and displayed in Fig. 14 (curve N_0).

(iv) Finally, the energy gap, which is needed in $R_S(T, a_S)$, is taken from the BCS theory, with $\Delta_0 = 2.15 k_B T_c$.

Going back to Fig. 18 and to the quantitative comparison between the experimental data and the theoretical predictions, it can generally be said that Eq. (5) (low-field limit) gives better agreement than Eq. (6) (high-field limit) except for $x_N \gtrsim 0.6$, as predicted from the value of r_c/a_N. Surprisingly, we see also that the divergence of curve SE,SE from the experimental one always begins when $r_c/a_N \simeq 1$. However, the latter fact may only be a coincidence, since r_c was estimated and not measured.

For $x_n \to 1$ the experimental points approach the curves MR,SE and MR,− together, while the curve SE,SE $\to 1$. This also is not unexpected, since the magnetoresistance becomes efficient only when N lamellas are wide enough (with respect to the cyclotron radius) to prevent the quasiparticles from being trapped inside. Of course, a smooth transition is observed between the ranges of validity of Eqs. (5) and (6), which describe limiting cases.

The two curves MR,− and MR,SE differ only in the calculation of the contribution of the S lamellas to the conductivity. As they differ little, the agreement just noted between theory and experiment reflects mainly the behavior of the quasiparticles in the *normal* lamellas. In considering the experimental uncertainties, which will now be discussed, we can conclude that the size effect picture of the thermal conductivity reduction in the N lamellas is confirmed by experiment over a wide range of the size-effect parameters. We emphasize that this result is obtained without any adjustable parameter in the theoretical expressions.

In each graph of Fig. 18, only the relative position of the different curves is well determined, due to the large uncertainty ($\pm 15\%$) affecting K_0 as a consequence of the poor definition of the mfp value. This is a disadvantage of the normalization by K_0. However, this uncertainty is common to all curves, and is not taken into account in the following

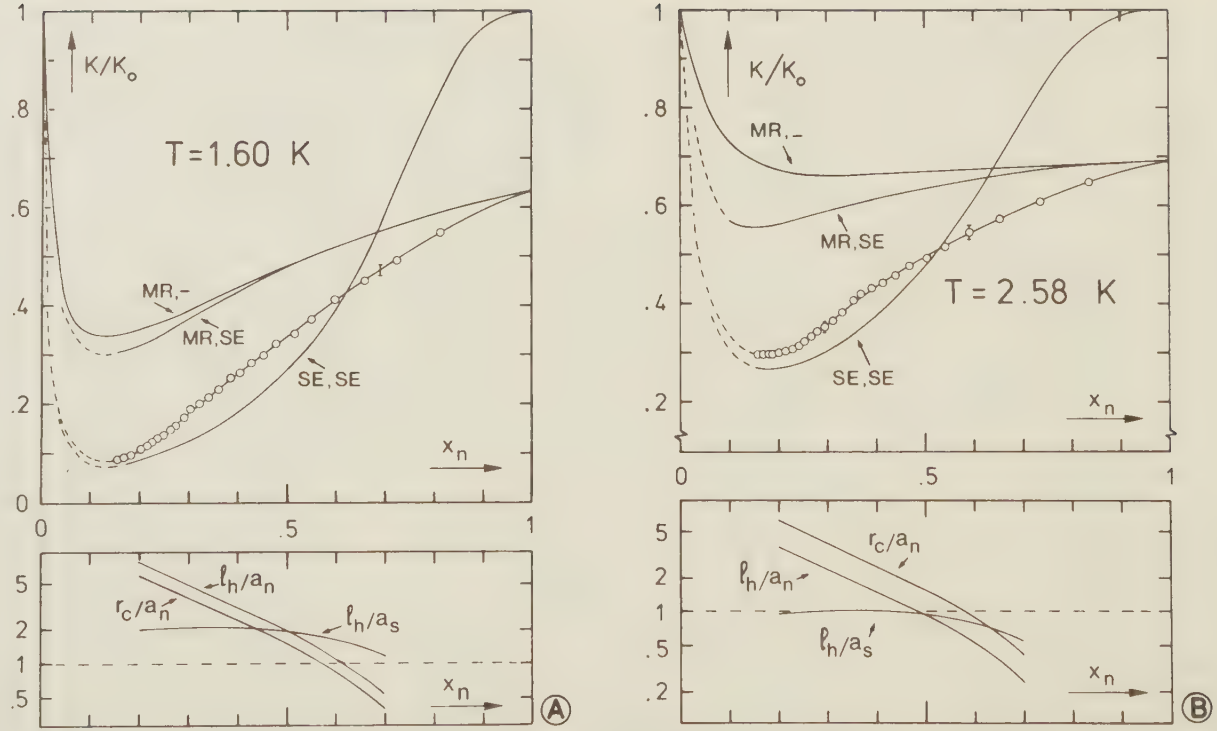

Fig. 18. Measured and calculated normalized thermal conductivities of the LLS in Pb 1. In each graph, the three theoretical curves are calculated using the parameter values displayed in the lower part. (MR,–) From Eq. (12) (simple model, magnetoresistance in the N lamellas, bulk conductivity in the S lamellas). (MR,SE) From Eq. (6), high-field limit (magnetoresistance in the N lamellas, size effect in the S lamellas). (SE,SE) From Eq. (5), low-field limit (size effect in both phases). K_0 is from Eq. (14) (trivial x_N dependence only), l_h is the electronic mfp for heat conduction in the *normal* lamellas, a_S and a_N are widths of the S and N lamellas, respectively, and r_c is the cyclotron radius in a critical field. See text.

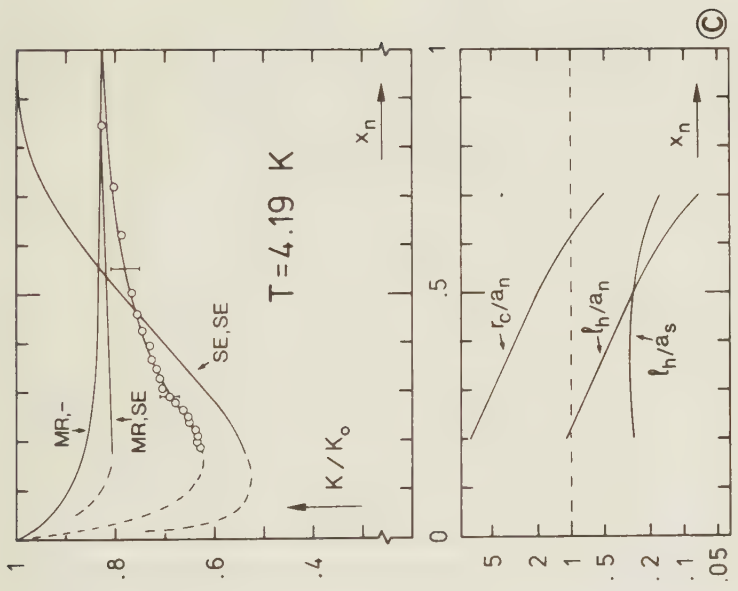

Fig. 18. Continued.

discussion. Normalization by K_0 reduces the uncertainty of the experimental points. Since K and K_0 are affected in the same way by the large error in x_N, the latter cancels out (in first approximation) in the ratio K/K_0. Another compensation occurs in the uncertainties of the mfp-dependent quantities, so that the additional error in the curve SE,SE—the only one to be essentially affected by the uncertainty on l_h—is only $\pm 5\%$ at 1.6 K and $\pm 15\%$ at 4.2 K.

Let us recall here that the (small) variations of several quantities along the sample are ignored in the theoretical calculations; in addition to the remarks of Section 5.1, let us mention that the period of the intermediate-state structure also varies by less than 10% along the sample in the worst case. This variation is not important in evaluating Eq. (5) (curve SE,SE) provided the mean values of the lamella widths a_N and a_S are used.* Finally, the experimental curves are slightly depressed due to the imperfections of the LLS at lower concentrations (Table V), and shifted to the left because the calculated x_N is a little bit smaller than the mean value of x_N along the sample, as already noted in Section 5.1.

It is concluded that for $x_N \lesssim 0.7$, the experimental data deviate significantly from curves MR,SE and MR,–, while there is fair agreement between the experimental data and the curves SE,SE in the x_N range where $r_c/a_N \gtrsim 1$.

We conclude this analysis of the size effect in lead with a few additional remarks.

(i) Lead is a strong coupling superconductor. This fact allowed us to concern ourselves only with the N lamellas in analyzing the results. In particular, we used for simplicity Eq. (5) and (6) in the whole temperature range 1.6–4.2 K, although they were derived assuming pure electronic heat conduction in both phases. Strictly speaking, the validity of these equations decreases as the temperature is lowered from 4.2 K, since the contribution of phonons to heat transport in the S phase gradually increases. However, at the same time the relative weight of the S lamellas in the intermediate-state conductivity is reduced, and the final result is not significantly altered by our simplified calculation procedure. Moreover, since the agreement with experiment is good, one may conclude that the strong coupling character of lead does not seem to modify Andreev's reflections of the quasiparticles at the interphase boundaries.[16]

(ii) The theoretical model assumes that all quasiparticles in both phases are reflected by the boundaries. There is little doubt that those coming from the N side are totally reflected in the temperature range

*It should be mentioned that, only for graphical reasons in Fig. 18, the function $a_N(x_N)$ was extrapolated above $x_N = 0.7$ using $a_N(x_N) = 0.1(1 - x_N)^{-2.6} a_{x_N = 0.375}$; this is a purely empirical formula verified for lead in our geometry in the range $0.3 \lesssim x_N \lesssim 0.7$.

studied, since $T < 0.8T_c$.[20] On the other hand, the number of quasiparticles in the S phase is small and little can be said of their behavior.

(iii) A further assumption of the theory is a spherical Fermi surface. This approximation seems also unimportant for lead.

In the whole analysis, the "ordinary" size effect due to the presence of the sample surfaces was implicitly neglected. In particular, the measured N-state thermal conductivity was introduced without correction into the theoretical expressions. Due to the large sample thickness chosen, the correction needed would have been small: 10% at 1.7 K, 5% at 2.5 K, and 1.5% at 4.2 K. However, it would have lead to an even better agreement between the curve SE,SE and experiment. This is because the ordinary size effect is not seen experimentally in the intermediate state in the low-field limit, as a consequence of the trapping of the quasiparticles which prevents them from reaching the sample surface.[52] (The sample thickness is ~ 10 times the lamella thickness). On the other hand, in the high-field limit where Andreev's size effect is inhibited by the magnetoresistance, the quasiparticles also do not reach the sample surface, because the electron trajectories are bent, thus also suppressing the ordinary size effect.

5.3. The Size Effect in Tin

The thermal conductivity of the LLS has also been measured in pure tin (sample Sn 1). The analysis of the results is similar to that reported in Sections 5.1 and 5.2. Therefore, in the present section we mainly discuss the differences between the two metals studied, lead and tin.

The most striking difference can be seen in Fig. 19, which is to be compared with Fig. 14. The thermal conductivity in the N and S phases is plotted v. the temperature.* Unlike in the case of lead, the conductivity has the same order of magnitude in the two phases. This is a consequence of the choice of the temperature range (which lies nearer to T_c) and of the fact that tin is a weak coupling superconductor (the decrease of K_S below T_c is not as sharp as in the case of lead). On the other hand, the magnetoresistance in the N phase is as strong as for lead.

Remembering that in tin, heat is carried mainly by electrons in both the N and S phases in the temperature range studied,[53] it appears that it is necessary to look also at the behavior of the excitations of the S phase in the calculation of the intermediate-state thermal conductivity.

The thermal conductivity of an intermediate-state LLS is given in Fig. 20. Its temperature dependence is stronger than in the case of lead. But the

*In Fig. 19, the conductivity is given as measured, without correction. First, tin is a compensated metal, like lead. Hence, the Righi-Leduc effect is negligible, as is seen from the optically obtained value ($\sim 12°$) of the Hall angle in a critical field.[50] Second, the "ordinary" size effect is small (15% at 1.6 K, 10% at 3 K), although more important than in lead.

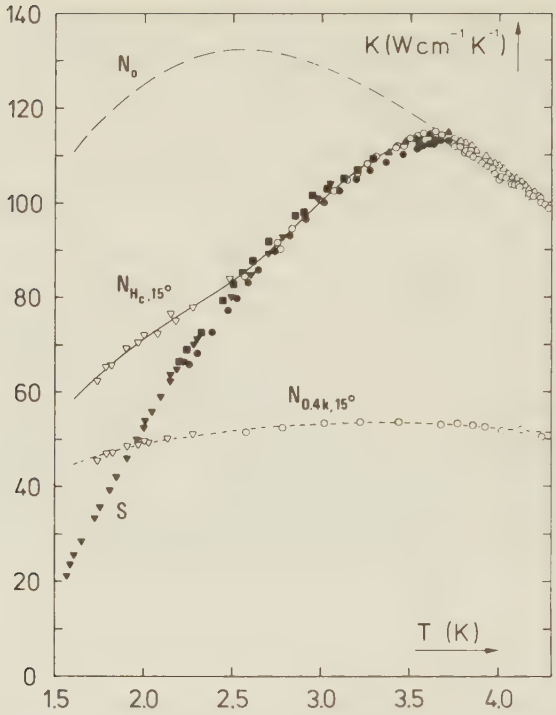

Fig. 19. Thermal conductivity of Sn 1. Here S denotes the frozen-flux free, superconducting state (closed symbols) and N the normal state (three curves, open symbols); the first index indicates the applied-field value [$H_c(T)$ or 0.41 kOe] and the second index the angle between the field and the heat current (15°). N_0 is the zero-field extrapolated normal-state conductivity. The data points are represented by symbols of different shape to distinguish between the successive thermometer calibrations used for the calculation of K. The thermometers were recalibrated after each warming up to room temperature.

thermal conductivity is relatively less reduced when the N phase concentration x_N decreases. The uncertainty on x_N is more important than in the case of lead, because of the occurrence of supercooling in tin (the definition of the critical field on the recorded traces is less accurate). In Fig. 20 another effect of the nonreproducibility of the intermediate-state structure can be seen: For large x_N, the curves are irregular. However, the range $x_N \gtrsim 0.7$ corresponds to incompletely formed LLS (Fig. 6A), and will not be considered further. The effect of the structural imperfections of the LLS is estimated to be the same in absolute value as in the case of lead. Indeed,

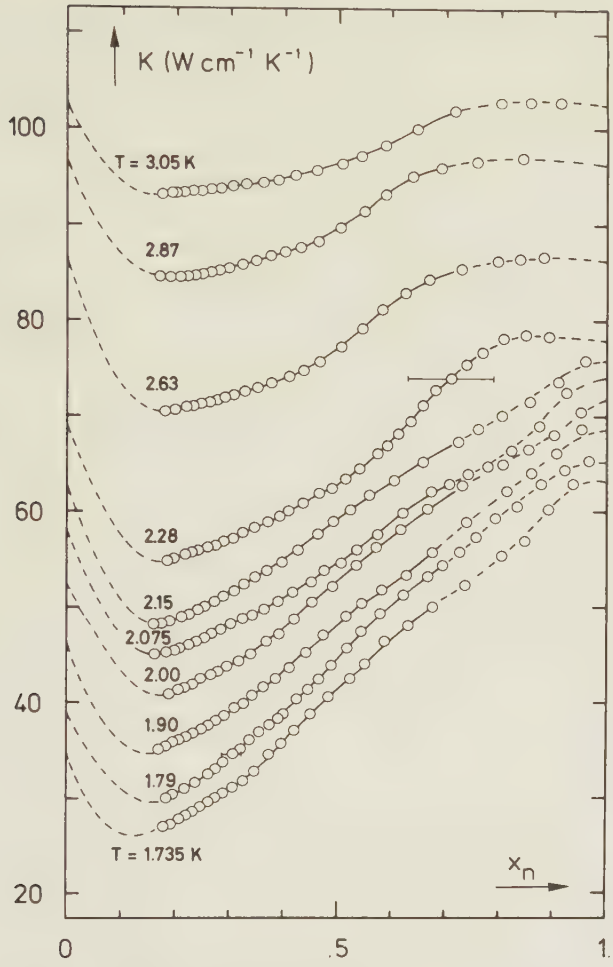

Fig. 20. Thermal conductivity of the LLS in Sn 1 at different temperatures and N-phase concentrations. Outside the range of existence of the LLS, the curves are represented by dashed lines connecting the S- and N-phase data ($x_N = 0$ or 1) to the curves obtained in the intermediate state. The experimental errors are discussed in the text.

the temperature jump per heat current density at an interphase boundary is $\sim 10^{-3}$ K cm^2/W for tin at $T = 1.7$ K,[18] i.e., of the same order of magnitude as for lead (Table V). However, when normalized with respect to the measured intermediate-state thermal resistivity, the effect of the structural imperfections is somewhat larger in tin than in lead.

The analysis of the thermal conductivity of the LLS is presented in Fig. 21 for two temperatures in the same way as for lead (Fig. 18). The way in which the values of the parameters used in the calculation of the theoretical curves were obtained—the values of the main parameters are again displayed in the lower part of each graph—will now be discussed.

(i) The lamella widths a_N and a_S are calculated from the concentration x_N and the period a, as previously. Here a is taken from Fig. 8 (dashed line). However, it has been necessary to extrapolate the available data up to $T = 3.05$ K. We have used Sharvin's result[9] $a \propto (1 - T/T_c)^{-1/4}$.*

(ii) The cyclotron radius in a critical field $r_c(T)$ is calculated as for lead, with four electrons per atom. As the field is lower, r_c is larger than in the case of lead. $r_c(0) = 0.40$ mm.

(iii) The determination of the mfp l_h is easier and more accurate than in the case of lead, since results on the normal-state thermal conductivity of our tin sample above T_c are available (Fig. 19). The validity of the extrapolation of the measured conductivity $K_N(T; T > T_c)$ below T_c to get $K_N(T, H = 0)$ is well established down to 2.7 K in our purity range.[53] Then $K_N(T, H = 0)$ gives the temperature dependence of l_h and the residual resistivity ρ_0 by the Wiedemann–Franz law. The absolute value of the mfp is readily obtained using the anomalous-skin-effect result[43] $\rho_0 l_0 = 1.05 \times 10^{-11} \Omega\,\mathrm{cm}^2$ to get its zero-temperature value: $l_0 = 0.36\ \mathrm{mm} \pm 10\%$. It should be noted that the T dependence of l_h is weaker in tin than in lead (only a factor two between 1.6 and 3.1 K), because tin has a higher Debye temperature.

(iv) The energy gap is taken from the BCS theory with $\Delta_0 = 1.75\, k_B T_c$.

(v) The angular dependence of $K_N[T, H_c(T)]$ was not studied systematically in tin. We postulated the $\sin^2 \beta$ law [Eq. (13)] and determined the absolute amplitude of the effect as follows. The ratio $(W_{15}/W_{90})_{H=H_c(T)}$ was measured at 2.1 K, and the result, 0.83, allowed us to assume a linear T dependence of this ratio.† A more accurate determination of the anisotropy of $K_N[T, H_c(T)] = 1/W_\beta$ was not required, since it follows from Eq. (13) that it is small: For instance, at 2.1 K, W_β changes by only 6% in the whole range $0.2 \leq x_N \leq 0.7$.

We now go to the quantitative comparison between the experimental data and the theoretical predictions (Fig. 21). It has first to be noted that the curves denoted by MR,− significantly deviate from the data points. Thus, in tin also, magnetoresistance in the N lamellas cannot explain the observed thermal conductivity reduction in the LLS.

*For graphical reasons only, we again extrapolated the curve $a_N(x_N)$ above $x_N \approx 0.75$, using an empirical relation verified for tin in our geometry in the range $0.65 \lesssim x_N \lesssim 0.75$ ($T = \mathrm{const}$): $a_N(x_N) = 0.475(1 - x_N)^{-0.93} a_{x_N = 0.375}$.

†Between 1.6 K and T_c, where, of course, $W_{15}/W_{90} = 1$ (since $H_c = 0$).

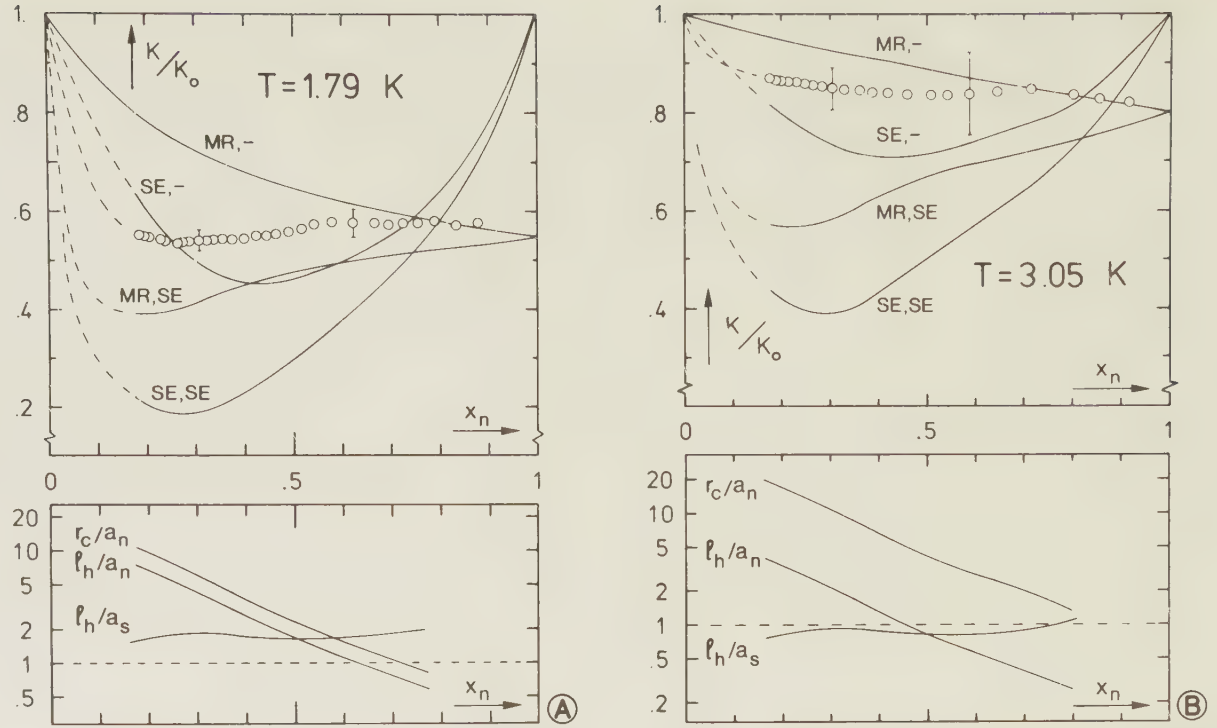

Fig. 21. Measured and calculated normalized thermal conductivities of the LLS in Sn 1. In each graph, the four theoretical curves are calculated using the parameter values displayed in the lower part. (MR,−) From Eq. (12) (simple model, magnetoresistance in the N lamellas, bulk conductivity in the S lamellas). (MR,SE) From Eq. (6), high-field limit (magnetoresistance in the N lamellas, size effect in the S lamellas). (SE,SE) From Eq. (5), low-field limit (size effect in both phases). (SE,−) From Eq. (15). K_0 is from Eq. (14) (trivial x_N dependence only), l_h is the electronic mfp for heat conduction in the *normal* lamellas, a_S and a_N are the widths of the S and N lamellas, respectively, and r_c is the cyclotron radius in a critical field. See text.

However, unlike in the case of lead, the theoretical expressions leading to the curves MR,SE and SE,SE are also unable to explain the observed conductivity reduction, although the values of the parameters look more favorable than in the case of lead. The r_c/a_N is larger; thus the validity range of the low-field limit [Eq. (5), curve SE,SE] should be more extended. Surprisingly, the largest deviations from the data points are just observed for this curve SE,SE. Only two minor points of the discussion of the results on lead are still valid here: (i) The experimental curve joins the curve MR,− when $r_c/a_N \lesssim 1$; (ii) the curve SE,SE and the experimental one intersect at $r_c/a_N \simeq 1$.

One reason for the discrepancy observed at lower concentrations x_N could be a wrong mfp value l_h. However, this is very improbable since l_h had to be approximately three times smaller to get agreement between the curve SE,SE and the experimental data. As already mentioned, l_h was determined rather accurately in tin, and we believe that the procedure used for this determination is the most convenient one in our case (see Section 5.2).

The discrepancy between theory and experiment is also too big to be explained by the fact that we neglected the longitudinal variations (at fixed applied field) of all quantities along the sample as well as the change in the mean temperature of the sample on reducing the applied field. The situation is less favorable in tin than in lead from this point of view, because of the proximity of the critical temperature. However, in the most unfavorable case (3.05 K) the x_N dependence of the measured conductivity is weak and the S- and N-state conductivities are of the same order of magnitude. The most important effect of the approximations made is thus a shift to the left of ~20% of the upper curve of Fig. 20 (the shift is correspondingly reduced at lower temperatures), while the comparison between theory and experiment (Fig. 21) is not affected.

Our opinion is that the discrepancy between theory and experiment does not originate in a wrong determination of the problem parameters. On the contrary, it should be due to some oversimplification in the theoretical model, which will now be discussed. We first note that in tin, unlike in lead, the contribution of the S lamellas to the conductivity of the LLS [second term in Eqs. (5), (6), and (12)] is of the same order of magnitude as the contribution of the N lamellas. This can be seen in Fig. 21 by comparing curve MR,SE [from Eq. (6)] to curve MR,− [from Eq. (12)], which only differ in the calculation of the contribution of the S phase. This contribution is important in tin, since $K_N[T, H_c(T)] \approx K_S(T)$ (Fig. 19).

Now, if one remembers that the previously obtained agreement between theory and experiment in the case of lead involved the size effect in the N lamellas only, it seems evident that, in looking for the origin of the

discrepancy in tin, one first has to reexamine the calculation of the contribution of the S lamellas.

A further reason for reconsidering the evaluation of the size effect in the S lamellas is the following. Neglecting in Eq. (5) (which corresponds to curve SE,SE) the size effect in the S lamellas, one gets

$$K(T, x_N) = x_N R_N(T, a_N) K_N(T, H = 0) + (1 - x_N) K_S(T) \qquad (15)$$

Of course, this procedure has no physical background. However, it is seen that the resulting curve SE,− (Fig. 21) is in better agreement with experiment than the curve SE,SE (although the x_N dependence exhibited by the curve SE,− is different from the experimental one). Hence, it is evident that the thermal conductivity reduction due to the size effect in the S lamellas has been *overestimated*, i.e., that the value of $R_S(T, a_S)$ we got in Eq. (3) is too small.

What could be the reasons for this? Evidently we cannot exclude that the well-known anisotropy of the transport properties of tin (see, e.g., Ref. 54) could be important in this context, although we used polycrystalline samples. We have neglected it totally, for simplicity. Second, we have also neglected the T dependence of the superconducting energy gap, which is important near T_c. But this second simplification modifies the final result by less than 2% in the temperature range studied, as was shown by evaluating again the theoretical expressions in taking into account the T dependence of $\Delta(T)$.*

The most drastic oversimplification in the calculation of the size effect should be the assumption that all the quasiparticles are reflected by the interphase boundaries. If this assumption seems to be correct for the quasiparticles of the N phase, since $T/T_c < 0.8$,[20] those of the S phase do not see a potential well, and the transmission probability is finite above the energy gap,[16,31] i.e., at energies that are still important in the calculation of the thermal conductivity. Thus, the number of quasiparticles being reflected is smaller than assumed in our calculation of $R_S(T, a_S)$, and the thermal conductivity of a S lamella with size effect is higher than indicated by this result. Indeed, this is just what is observed experimentally.

Looking further at the transmission probability of an interphase boundary, or of an interphase-boundary pair, we note that this probability can indeed be very high just above the gap. In a calculation including the

*The value of $K_S(T, a_S)$ given by Eq. (2) is increased by 9% at 1.79 K and 55% at 3.05 K. However, the relevant quantity $R_S(T, a_S)$, Eq. (3), is increased by only 0.3% and 1.6%, respectively. On the other hand, the contribution of the N lamellas is, of course, unchanged. Finally, the effect of taking into account the T dependence of $\Delta(T)$ is a small increase in the thermal conductivity calculated by Eqs. (5) and (6); this increase amounts to 1.5% in the worst case ($x_N = 0.175$, $T = 3.05$ K), and is correspondingly smaller at higher concentration or lower temperature.

possibility for quasiparticles to tunnel through the central lamella of a S–N–S or N–S–N sandwich (the so-called "Shikin geometry"), Demers and Griffin[31] obtained an oscillating transmission probability, with many peaks above the gap. At those peaks, the probability is equal to unity. By rescaling their Fig. 3 according to our lamella width $a_S \approx 10^{-2}$ cm (see Fig. 8), the peaks are seen to accumulate near Δ. The energy interval between two successive peaks is 100 times shorter than indicated in the referenced figure. Evidently, these peaks could also have a nonnegligible effect in the calculation of the thermal conductivity of the LLS in the case of tin.

6. CONCLUSION

The thermal conductivity of a longitudinal lamellar structure (LLS) has been measured in lead and tin in the temperature ranges 1.6–4.2 and 1.7–3.05 K, respectively. The structure was studied optically in a separate experiment reproducing the conditions of the thermal conductivity measurements. In particular, the range of existence and the period of the LLS were determined. The optical study of the structure was also decisive to ensure that the effect observed when the heat current is perpendicular to the interphase boundaries does not interfere with the size effect we looked for, although the former can be much greater than the latter. Other parameters, such as the concentration of the N phase in the LLS and the electronic mfp were calculated from auxiliary measurements of the thermal and electrical conductivities. This, together with measurements of the N and S state thermal conductivity of the investigated samples, enabled a detailed comparison between the experimental results and the theoretical model of the thermal conductivity of the LLS described in Section 2.

The situation turned out to be very different in the two metals studied. In lead, heat flows essentially in the N lamellas, and this fact simplifies the interpretation of the data, since any effect in the S phase as well as phonon conduction can be ignored. The experimental results can be explained using Andreev's model of the size effect in the N lamellas (however, with an extension to a finite mfp and a restriction to a spherical Fermi surface). Thus, the quasiparticle trapping picture in a N lamella between two parallel interphase boundaries is essentially confirmed over a wide range of the parameter values. This in turn gives indirect support—if any is still necessary—to the peculiar reflection mechanism of the quasiparticles at a normal–superconductor interphase boundary, which was first described 1964 by Andreev.[16]

In tin the results are more difficult to interpret, as heat transport by *all* the lamellas of the LLS—S lamellas as well as N lamellas—must be considered. In what concerns the behavior of the quasiparticles in the N lamellas

in the case of tin, there is no reason to doubt of Andreev's description, which correctly describes the situation in lead. However, the validity of this model could not be established in tin because of some difficulty in the calculation of the contribution of the S lamellas to the thermal conductivity. Indeed, the situation arising in a S lamella is much more complicated than that in a N lamella, although conduction by phonons can be neglected in tin above 1.7 K. The complications arise from the reflection coefficient of the excitations by an interphase boundary, which is no longer equal to unity. The excitations are partly reflected, which again gives rise to trapping in the lamella, and partly transmitted. The latter fact was ignored in our simple calculation, and this should be the principal reason for the discrepancy between the theoretical model and our experimental results.

Qualitative comparison indicates that it should be possible, in principle, to explain also in tin the anomalously small thermal conductivity of the LLS by starting from Andreev's size-effect picture. However, new theoretical developments are needed in the case of heat conduction by all the lamellas of the LLS. The calculation is much more complicated since one can no longer calculate separately the contributions of the lamellas of both types. In the case of tin, a further complication could be the necessity of also taking into account the high anisotropy of the transport properties of this metal.

ACKNOWLEDGMENTS

We are thankful to Prof. F. Rothen, Dr. E. Posada, Dr. W. M. MacInnes, and Dr. R. Ehrat for many illuminating discussions. The magnetooptical observations of the intermediate-state structure were made using Dr. P. Laeng's experimental device; we express to him our gratitude for this contribution and for interesting discussions. We thank the technical staff of our laboratory for their assistance.

REFERENCES

1. J. K. Hulm, *Phys. Rev.* **90**, 1116 (1953); C. A. Renton, *Phil. Mag.* **46**, 47 (1955).
2. N. V. Zavaritskii, *Zh. Eksp. Teor. Fiz.* **38**, 1673 (1960) [*Sov. Phys.—JETP* **11**, 1207 (1960)].
3. P. Wyder, *Phys. Kondens. Materie* **3**, 292 (1965).
4. K. Mendelssohn and J. L. Olsen, *Phys. Rev.* **80**, 859 (1950).
5. S. J. Laredo and A. B. Pippard, *Proc. Camb. Phil. Soc.* **51**, 368 (1955).
6. F. H. J. Cornish and J. L. Olsen, *Helv. Phys. Acta* **26**, 369 (1953).
7. J. L. Olsen, A. Waldvogel, and P. Wyder, *Helv. Phys. Acta* **39**, 361 (1966).
8. S. Strässler and P. Wyder, *Phys. Rev. Lett.* **10**, 225 (1963).
9. Yu. V. Sharvin, *Zh. Eksp. Teor. Fiz.* **33**, 1341 (1957) [*Sov. Phys.—JETP* **6**, 1031 (1958)].
10. T. E. Faber, *Proc. Roy. Soc. Lond. A* **248**, 460 (1958).
11. F. Haenssler and L. Rinderer, *Helv. Phys. Acta* **38**, 448 (1965).

12. H. Träuble and U. Essmann, *Phys. Stat. Sol.* **18**, 813 (1966).
13. R. P. Huebener, R. T. Kampwirth, and V. A. Rowe, *Rev. Sci. Instr.* **41**, 722 (1970).
14. H. Kirchner, *Phys. Stat. Sol.* (*a*) **4**, 531 (1971).
15. P. Laeng and L. Rinderer, *Helv. Phys. Acta* **46**, 8 (1973).
16. A. F. Andreev, *Zh. Eksp. Teor. Fiz.* **46**, 1823 (1964) [*Sov. Phys.—JETP* **19**, 1228 (1964)].
17. A. F. Andreev, *Zh. Eksp. Teor. Fiz.* **47**, 2222 (1964) [*Sov. Phys.—JETP* **20**, 1490 (1965)].
18. A. J. Walton, *Proc. Roy. Soc. Lond. A* **289**, 377 (1965).
19. A. F. Andreev, *Zh. Eksp. Teor. Fiz.* **51**, 1510 (1966) [*Sov. Phys.—JETP* **24**, 1019 (1967)].
20. I. L. Landau, *Zh. Eksp. Teor. Fiz. Pisma* **11**, 437 (1970) [*Sov. Phys.—JETP Lett.* **11**, 295 (1970)].
21. A. B. Pippard, J. G. Shepherd, and D. A. Tindall, *Proc. Roy. Soc. Lond. A* **324**, 17 (1971).
22. A. F. Andreev, *Zh. Eksp. Teor. Fiz.* **49**, 655 (1965) [*Sov. Phys.—JETP* **22**, 455 (1966)].
23. N. V. Zavaritskii, *Sov. Phys.—JETP Lett.* **2**, 106 (1965).
24. W. J. Tomasch, *Phys. Rev. Lett.* **15**, 672 (1965).
25. W. J. Tomasch, in *Tunneling Phenomena in Solids*, E. Burstein and S. Lundqvist, eds. (Plenum Press, New York, 1969), Chapter 23.
26. I. P. Krylov and Yu. V. Sharvin, *Zh. Eksp. Teor. Fiz. Pisma* **12**, 102 (1970) [*Sov. Phys.—JETP Lett.* **12**, 71 (1970)].
27. I. P. Krylov and Yu. V. Sharvin, *Zh. Eksp. Teor. Fiz.* **64**, 946 (1973) [*Sov. Phys.—JETP* **37**, 481 (1973)].
28. J. M. Suter, F. Rothen, and L. Rinderer, *J. Low Temp. Phys.* **20**, 429 (1975).
29. J. M. Suter and L. Rinderer, in *Proc. of the 14th Int. Conf. on Low Temperature Physics*, M. Krusius and M. Vuorio, eds. (North-Holland, Amsterdam, 1975), Vol. 2, p. 133.
30. L. D. Landau, *Phys. Z. Sowjet.* **11**, 129 (1937).
31. J. Demers and A. Griffin, *Can. J. Phys.* **49**, 285 (1971).
32. L. P. Kadanoff and P. C. Martin, *Phys. Rev.* **124**, 670 (1961).
33. J. Bardeen, G. Rickayzen, and L. Tewordt, *Phys. Rev.* **113**, 982 (1959).
34. B. Knecht, J. M. Suter, and L. Rinderer, *J. Low Temp. Phys.* **22**, 673 (1976).
35. A. C. Anderson, *Rev. Sci. Instr.* **39**, 605 (1968).
36. J. B. Sousa, *Cryogenics* **8**, 105 (1968).
37. J. R. Clement and E. H. Quinnel, *Rev. Sci. Instr.* **23**, 213 (1952).
38. J. M. Suter, P. Laeng, and L. Rinderer, *Helv. Phys. Acta* **46**, 5 (1973).
39. P. Laeng, F. Haenssler, and L. Rinderer, *J. Low Temp. Phys.* **4**, 533 (1971).
40. D. E. Farrell, R. P. Huebener, and R. T. Kampwirth, *Solid State Comm.* **11**, 1647 (1972).
41. P. Laeng and L. Rinderer, to be published.
42. A. L. Schawlow, *Phys. Rev.* **101**, 573 (1956).
43. R. G. Chambers, *Proc. Roy. Soc. Lond. A* **215**, 481 (1952).
44. J. J. Krempasky and D. E. Farrell, *Phys. Rev. B* **9**, 2894 (1974).
45. I. L. Landau and Yu. V. Sharvin, *Phys. Rev. B* **13**, 1359 (1976).
46. E. M. Lifshitz and Yu. V. Sharvin, *Dokl. Akad. Nauk. USSR* **79**, 783 (1951).
47. A. Bodmer, *Phys. Stat. Sol.* (*a*) **19**, 513 (1973).
48. A. Bodmer, U. Essmann, and H. Träuble, *Phys. Stat. Sol.* (*a*) **13**, 471 (1972).
49. J. A. Osborn, *Phys. Rev.* **67**, 351 (1945).
50. F. Haenssler and L. Rinderer, *Helv. Phys. Acta* **40**, 659 (1967).
51. J. Higgins, S. H. Tang, and P. A. Schroeder, *J. Low Temp. Phys.* **24**, 519 (1976).
52. I. P. Krylov, I. L. Bronevoi, and Yu. V. Sharvin, *Zh. Eksp. Teor. Fiz. Pisma* **19**, 588 (1974) [*Sov. Phys.—JETP Lett.* **19**, 306 (1974)].
53. A. M. Guénault, *Proc. Roy. Soc. Lond. A* **262**, 420 (1961).
54. J. E. Gueths, C. A. Reynolds, and M. A. Mitchell, *Phys. Rev.* **150**, 346 (1966).